Eidgenössische Technische Hochschule Zürich
Swiss Federal Institute of Technology Zurich

PAUL SCHERRER INSTITUT

An investigation into the robustness of proton therapy treatments against rotational and translational setup errors

Semester Project

Author: Alina – Mihaela Paunoiu

Supervisors: Prof. Dr. Antony J. Lomax, Dr. Giovanni Fattori

January 2023

Contents

Abstract

With robust treatment planning, optimal coverage of the clinical target volume (CTV) and sparing of the organs at risk (OAR) are maintained, despite delivery uncertainties. This is especially important in proton therapy, as treatments are very sensitive to such errors, which lead to dose degradation. Although range uncertainties are one of the most investigated aspects of robust planning, spatial misalignments should also be considered. Most often, translational shifts of the patient are assessed in clinical settings. In this project, a pipeline was developed to account for rotational positioning uncertainties and compared their magnitudes to translational ones. This was performed on a set of head and neck cancer patients, treated at the Center for Proton Therapy (CPT) at the Paul Scherrer Institute (PSI). Dose discrepancies were evaluated for both translational and rotational uncertainty scenarios and showed that proton treatments of this patient site are more sensitive to translations than rotational uncertainties. Thus, the results of the simulations can serve as a way forward in terms of improving plan robustness, in order to ensure that the patient receives an optimal treatment.

1. Introduction

Radiation therapy in the form of proton therapy is an efficient treatment modality when it comes to killing cancer cells, by delivering a high dose to the target volume while sparing surrounding critical structures [1,2]. This project focuses on a topic of general interest in proton therapy, namely assessing treatment plan robustness, a measure of the sensitivity of a radiation treatment to inevitable and residual patient positioning errors [1].

The goal of the project is to investigate the sensitivity of proton treatment plans to rotational positioning uncertainties and compare the magnitudes of their effects to those resulting from translational errors. In order to achieve this, a pipeline has been developed and tested through a series of dose simulations. A set of proton therapy head and neck treatments is selected from the database of delivered plans at the Center for Proton Therapy (CPT) at the Paul Scherrer Institute (PSI). Uncertainties in the treated geometry are simulated by transforming the planning CTs and recalculating the dose. Standard robustness analysis is also performed by considering rigid translations of the patient in relation to the beam, for the same cases. Dose discrepancies, with respect to the nominal plan, are evaluated for the two, using dose distributions, dose – volume histograms (DVH), the worst – case distribution and error bar – based analysis to determine the more robust approach [3].

The project report is structured as follows: section 2 describes the general concept of plan robustness and the impact of uncertainties on the treatment, section 3 details the setup error modelling procedures and section 4 presents the results. The report concludes with a discussion in section 5.

2. Robustness in proton therapy

Protons are charged particles; their energy deposition is characterised by the Bragg curve as they penetrate the tissues. As protons travel at deeper depths, they slowly lose energy, mainly by interacting with orbiting electrons. Therefore, their velocity is reduced and the deposited energy correspondingly increases. The dose deposition reaches a peak by the end of the proton range, where they slow down and stop. The sharp fall – off of the dose at the distal end is the reason why proton therapy is so effective in sparing organs at risk (OAR) [4,5]. Through the spot scanning technique, individual Bragg peaks are placed within the target by magnetic deflection of the proton beam, in energy layers.

The precision and accuracy of treatment planning and delivery are affected by a number of uncertainties. The range of the proton beam depends on its initial energy and the tissues it crosses. Therefore, it is generally hard to determine precisely where protons stop in the patient. Over the patient population, range uncertainty is randomly distributed, but it can become systematic for the individual cases, due to errors in the conversion from Hounsfield units (HU) of a patient's CT to relative proton stopping power (SP), for example. Such a systematic error can propagate throughout the whole treatment [6,7,8]. Other sources of range uncertainty include CT artifacts or variations in patient anatomy, such as weight loss or weight gain [7,9].

When density heterogeneities are present, like in the case of the complex anatomy of a patient's head, it can lead to dose degradation. If the patient shifts, coverage of the target may not be so well preserved anymore, both inside the target and at the boundary. This is due to the mismatch of dose contributions from individual beams, making proton therapy highly sensitive to errors [1,4,9]. This makes correct patient positioning and treatment beam alignment important. In the image guided radiotherapy paradigm, daily imaging is used to navigate the

patient and replicate the geometry of the treatment planning CT. Nevertheless, residual setup uncertainties will still remain and are subject to random errors [7,10].

Optimal treatment quality needs to be ensured and, for this, several strategies can be adopted to assess the robustness of proton treatment plans to uncertainties. First, it should be known that physical quantities should generally be associated with an error bar to account for any possible variation. In fact, as M. Goitein described in his paper, "at every point within the patient there is in fact a range of possible doses which may be delivered" [11]. Furthermore, he proposed the use of safety margins to account for patient positioning errors, which has become standard procedure in radiation therapy [11].

In clinics, setup errors are modelled by generating a number of error scenarios to evaluate the effects of translational shifts of the patient relative to the beam and recalculating the corresponding plans, either considering a single fraction delivery or a fractionated treatment [7]. The worst–case dose distribution was adopted by Lomax *et. al.* (2001) to evaluate plan robustness. This is done by creating a lower bound on the plan quality by combining multiple dose distributions into one, which stores the minimum dose values of voxels inside the target volume, across all distributions [12]. In addition, one can incorporate the best–case dose distribution, which applies the same concept, but the resulting dose distribution stores the maximum dose values of the voxels inside the target volume instead, serving as the upper bound on plan quality. However, this approach proves to be unphysical, since every voxel would be treated independently for each treatment error scenario [7,13,14].

Albertini *et. al.* (2011) described the error bar distributions as a tool to display dose variations resulting from the combined treatment error scenarios mentioned previously [1]. This is performed by subtracting the maximum dose values by the minimum dose values in each voxel across all distributions. Moreover, error bar volume histograms (EVH) can be used to evaluate the robustness of the plans. They are extracted analogously to DVH for each region of interest (ROI) and represent the percentage volume for which the error bar has a minimum magnitude [1,7,14].

3. Methods

The effect of setup uncertainties was simulated for single fraction treatment [7]. The planning CT images have been processed using open – source image processing software libraries to implement the 6 degrees – of – freedom (DOF) transformations [3]. The proton treatment plans were generated using the in – house treatment planning software (TPS) at PSI, FIonA.

The planning CT and corresponding structure set were provided, with a resolution of $0.98 \times 0.98 \times 2$ mm. The CT images were resampled on an isotropic grid at $1 \times 1 \times 1$ mm resolution, by linear interpolation of voxel intensities [3]. Resulting contours have been post–processed using a 2D filter that corrects for the artifacts resulted from the resampling procedure. The treatment couch was also removed in the process. The plans were then re – optimised.

3.1. Patient data

Three clinically relevant cases were included in this study, which consist of tumours in the head and neck region. Each has been planned using single field uniform dose (SFUD), such that the combined treatment fields are optimised to individually deliver a homogenous dose to the target volume [1].

Dose calculation in the TPS was performed using a ray casting pencil beam model which can simulate how the dose distribution is affected by tissue heterogeneities [5,7].

The prescribed treatment doses that were delivered to the three patients were between 1.8 Gy_{RBE} – 2 Gy_{RBE}, with a radio biological effectiveness (RBE) of 1.1 This is shown in table 1, which also contains, for each patient, the number of fields that were used for the treatment, as well as the volume of CTV that was irradiated. The patients were immobilised using a bite – block.

Table 1: Selected cases and patient data

Cases	Number of treatment fields	CTV Volume (cm^3)	Mean dose (range) (Gy_{RBE})
1	2	37.45	1.8 (1.71 – 1.87)
2	4	174.40	1.82 (0.98 – 2.04)
3	4	106.57	2 (1.63 – 2.16)

3.2. Modelling the setup errors

Figure 1 illustrates the general workflow that was designed to model the setup errors.

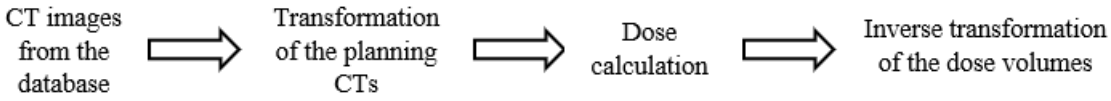

Figure 1: Pipeline for generating setup uncertainties

Transformations were applied to the planning CTs such that setup error scenarios were generated. These consisted of rotations and translations of the patient with respect to the treatment isocentre. In terms of rotational positioning uncertainties, the roll, pitch and yaw setup errors (about the x, y and z axes) were implemented with a magnitude of 1º [3]. Displacements were performed considering the 3 anatomical axes of the patient (±x, ±y, ±z) and 4 diagonal axes (±x, ±y, ±z) [7]. The combined effect of the random errors along the major anatomical axes of the patient (left – right, anterior – posterior and cranial – caudal), σ, was modelled as if inside of a sphere bounded by an 85% confidence limit (figure 2). The radius is given as the quadratic sum of random errors. The resulting value was used to transform the planning CTs used for dose calculation [1,7,13].

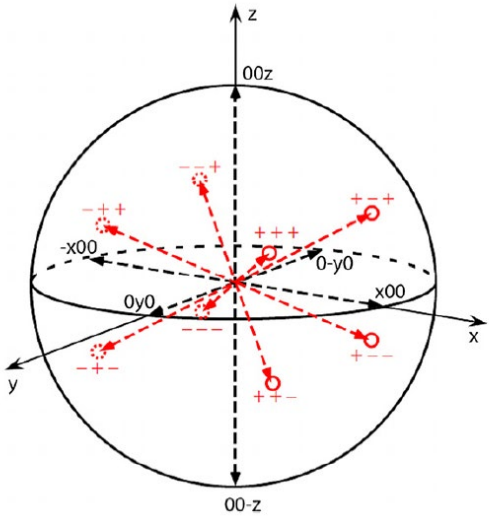

Figure 2: Schematic for setup error simulations [1]

As a result, the translations applied to the planning CTs had a magnitude of 1.76 mm (corresponding to 1.44σ), based on data recorded by Lowe *et. al.* (2016). The 85% confidence level was recommended by Goitein (1983) and is used in clinical practice at PSI [7,15].

For each patient, a total of 28 treatment error scenarios have been assessed (14 rotations and 14 translations). The plans for the transformed CT have been calculated for each scenario. The resulting dose volumes were then transformed back to realign to the contours of the nominal plan [3].

3.3. Plan dose evaluation

The impact of rotational and translational positioning uncertainties has been visualised in the form of dose distributions and analysed using dose – volume histograms (DVH) [7]. Larger DVH bands are indicative of an increased sensitivity of the ROI to delivery uncertainties [16].

The worst–case and best–case distributions were studied individually for rotations and translations. This was done by assigning the minimum dose values in a given voxel across all error scenarios. The same principle was applied for the maximum dose values. The resulting DVH bands represent the lower and upper bound on the plan quality with respect to the nominal plan. Using the newly combined maximum and minimum dose distributions, computing the difference between them generates an error bar (eq. 1) [1,7,14]:

$$\Delta D_{\sigma}^{i} = \mathrm{Max}\left(D_{+x}^{i}, D_{-x}^{i}, \dots, D_{-z}^{i}, D_{nom}^{i}\right) - \mathrm{Min}\left(D_{+x}^{i}, D_{-x}^{i}, \dots, D_{-z}^{i}, D_{nom}^{i}\right) \qquad (1)$$

In equation (1), ΔD_{σ}^{i} is the dose grid point *i* in the resulting error distribution, D_{+x}^{i} is the dose value at point *i* for the recalculated plan in the positive x – direction error scenario and D_{nom}^{i} is the dose grid point *i* for the nominal plan [1]. Error bar dose distributions were visualised to assess the percentage dose differences for both translational and rotational positioning uncertainties. In addition, EVH bands were calculated similarly to DVH, to determine how robust the treatment plan is in a reliable way: the closest the histogram is to zero, the more robust the plan is. The magnitude of the error was computed as percentage difference from the prescribed dose [1,14,17].

4. Results

In this section, the results for each patient will be displayed, namely dose distributions, DVH, the worst – case and best – case representation, as well as error bar visualisation and evaluation through dose difference distributions and EVH. An exemplary set of transformation parameters has been chosen, namely: (0º, 0º, ±1º), (+ 1º, + 1º, +1º) and (− 1º, − 1º, −1º) rotational errors, as well as (± 1.76, 0, 0), (+ 1.76/√3, + 1.76/√3, + 1.76/√3) and (−1.76/√3, −1.76/√3, −1.76/√3) translational displacements.

4.1. Dose distributions

Figures 3 – 8 show the nominal dose distribution, as well as the simulated dose distributions for the magnitudes of the positioning uncertainties mentioned in section 4. For each patient, the dose distributions are normalised such that the dose bands show the percentage dose relative to the prescribed dose to the target volume [7].

4.1.1. Patient 1

The dose distributions for the first patient are shown below: figure 3 is representative of the rotational errors and figure 4 corresponds to scalar shifts (see Appendix for additional rotations: (0º, ±1º, 0º), (±1º, 0º, 0º), (± 1º, ± 1º, ±1º) (figures 23, 24) and translations:

(0,±1.76, 0), (0, 0, ± 1.76), (±1.76/√3, ± 1.76/√3, ± 1.76/√3) (figures 25, 26)). For a clear visualisation, only dose values above 30% of the prescribed dose to the target volume are displayed.

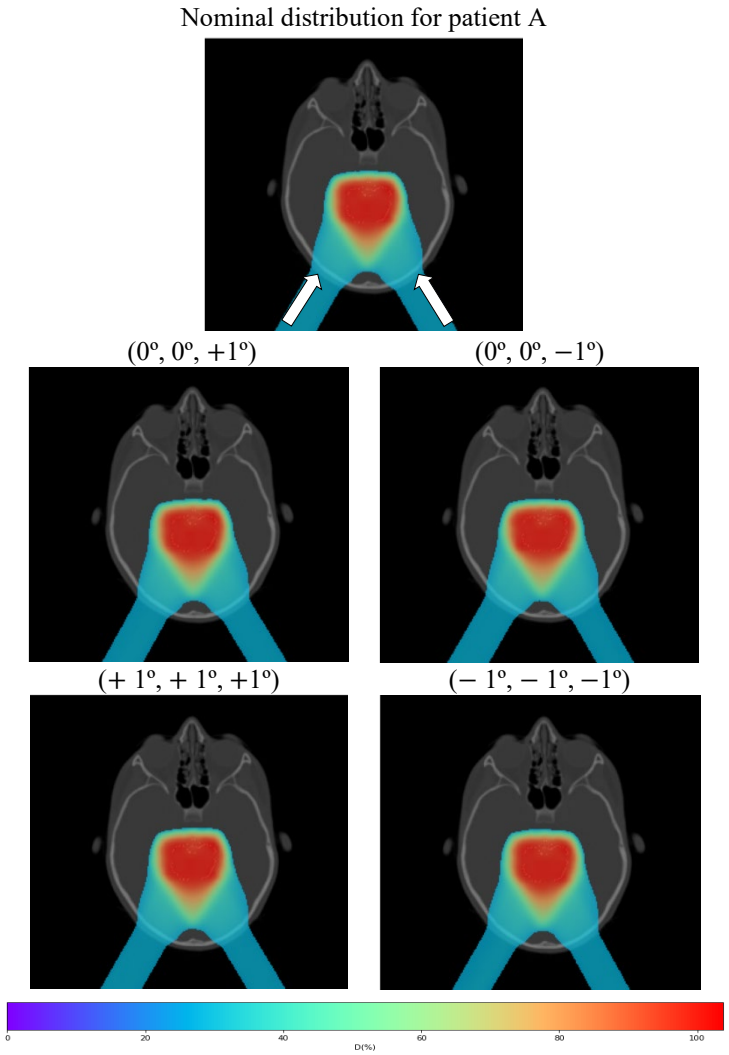

Figure 3: Axial slices for the first patient showing the nominal dose distribution (top), with arrows indicating the beam angles, and the resulting dose distributions for (0º, 0º, ±1º) (middle) and (± 1º, ± 1º, ±1º) (bottom) rotational errors. The CTV and the brainstem are delineated. Dose bar shows the percentage dose relative to the prescribed dose to the target volume, shown on the same scale for all dose distributions.

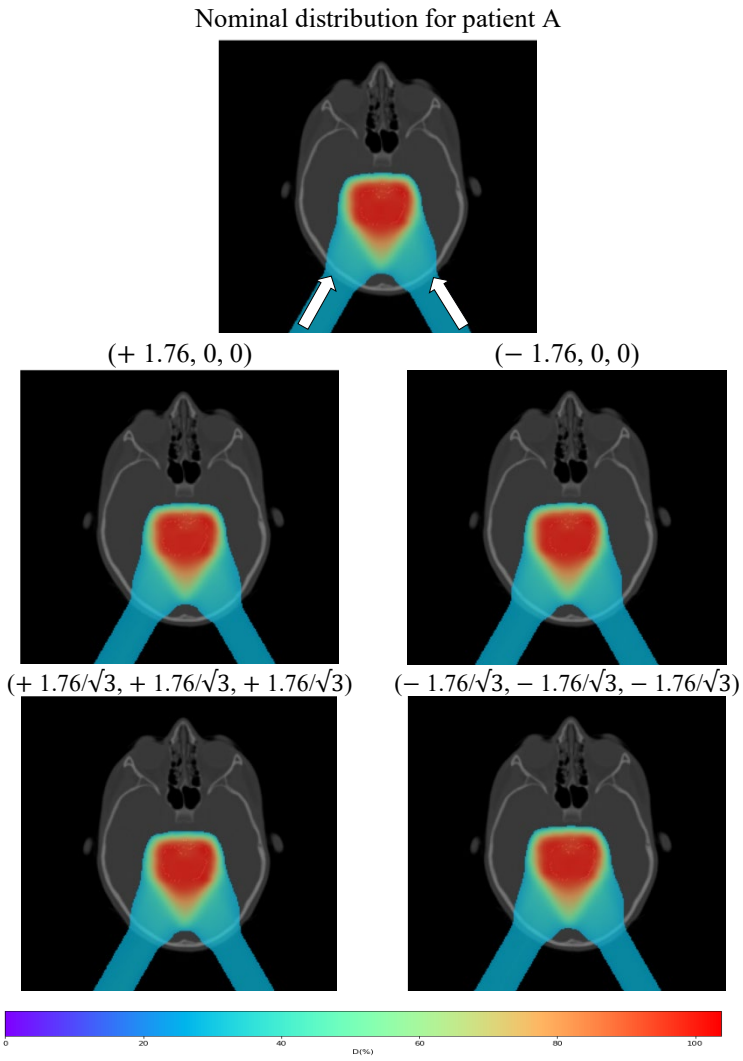

Figure 4: Axial slices for the first patient showing the nominal dose distribution (top), with arrows indicating the beam angles, and the resulting dose distributions for (± 1.76, 0, 0) (middle) and (±1.76/√3, ± 1.76/√3, ± 1.76/√3) (bottom) translations. The CTV and the brainstem are delineated. Dose bar shows the percentage dose relative to the prescribed dose to the target volume, shown on the same scale for all dose distributions.

4.1.2. Patient 2

The dose distributions for the second patient are displayed below: figure 5 is representative of the rotational setup errors and figure 6 shows the applied shifts (see Appendix for additional rotations: (0º, ±1º, 0º), (±1º, 0º, 0º), (± 1º, ± 1º, ±1º) (figures 27, 28) and translations: (0, ± 1.76, 0), (0, 0, ± 1.76), (±1.76/√3, ± 1.76/√3, ± 1.76/√3) (figures 29, 30)).

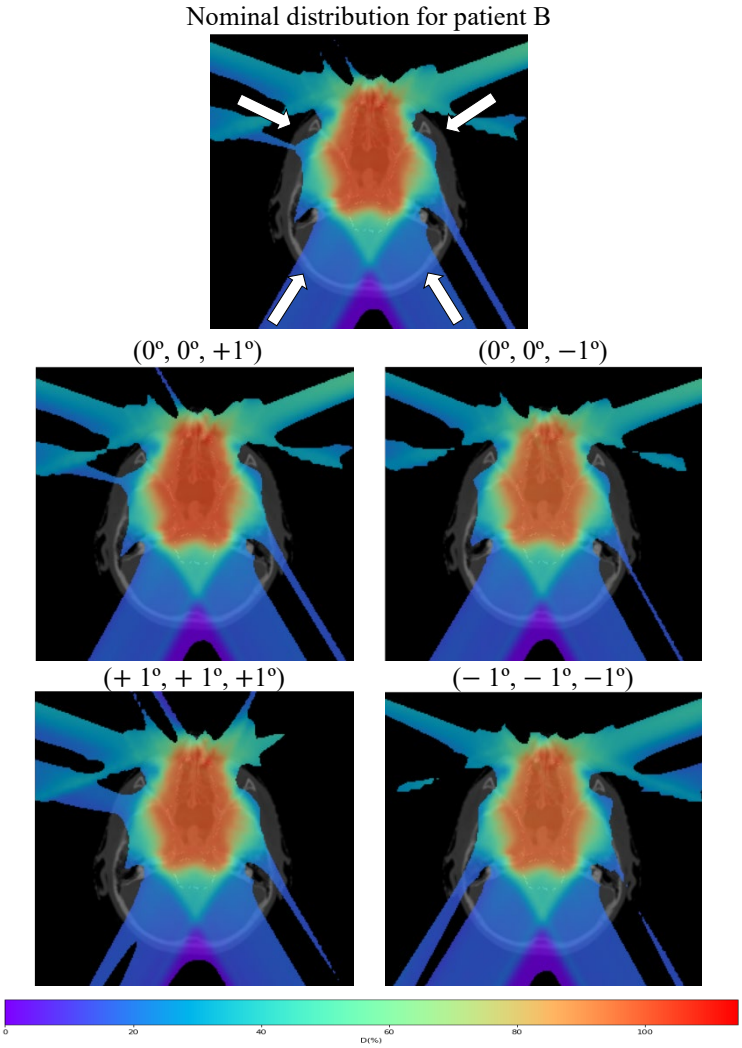

Figure 5: Axial slices for the second patient showing the nominal dose distribution (top), with arrows indicating the beam angles, and the resulting dose distributions for (0º, 0º, ±1º) (middle) and (± 1º, ± 1º, ±1º) (bottom) rotational errors. The CTV and the brainstem are delineated. Dose bar shows the percentage dose relative to the prescribed dose to the target volume, shown on the same scale for all dose distributions.

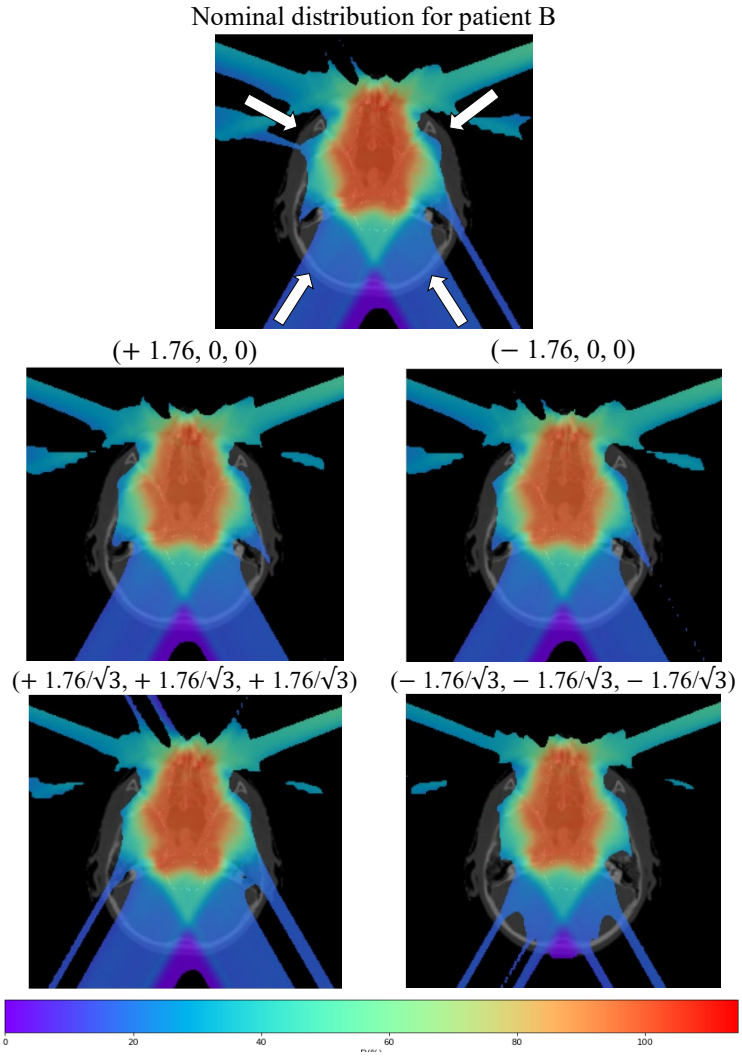

Figure 6: Axial slices for the second patient showing the nominal dose distribution (top), with arrows indicating the beam angles, and the resulting dose distributions for (± 1.76, 0, 0) (middle) and (±1.76/√3, ± 1.76/√3, ± 1.76/√3) (bottom) translations. The CTV and the brainstem are delineated. Dose bar shows the percentage dose relative to the prescribed dose to the target. volume, shown on the same scale for all dose distributions, for comparison.

4.1.3. Patient 3

For the third patient, the effects of rotational errors can be visualised in figure 7 and those of translational uncertainties in figure 8 (see Appendix for additional rotations: (0º,±1º,0º), (±1º, 0º, 0º), (± 1º, ± 1º, ±1º) (figures 31, 32) and translations: (0, ± 1.76, 0), (0,0,±1.76), (±1.76/√3, ± 1.76/√3, ± 1.76/√3) (figures 33, 34)). Dose values above 35% of the prescribed dose to the target volume are displayed.

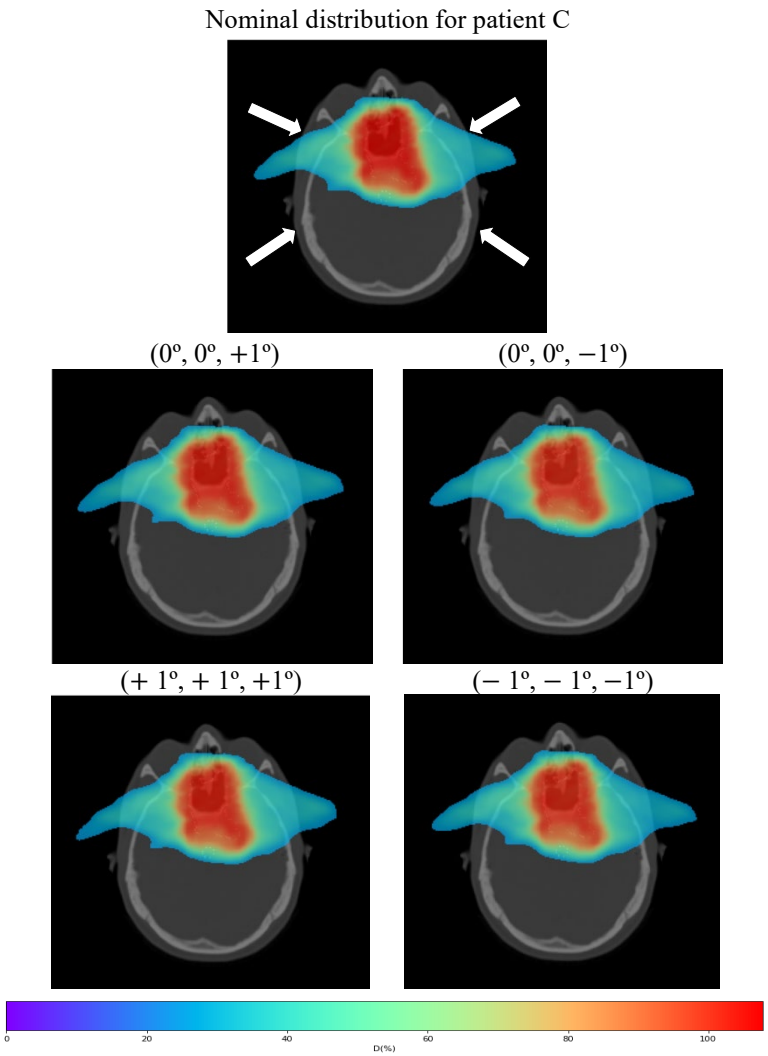

Figure 7: Axial slices for the third patient showing the nominal dose distribution (top), with arrows indicating the beam angles, and the resulting dose distributions for (0º, 0º, ±1º) (middle) and (± 1º, ± 1º, ±1º) (bottom) rotational errors. The CTV and the brainstem are delineated. Dose bar shows the percentage dose relative to the prescribed dose to the target volume, shown on the same scale for all dose distributions, for comparison.

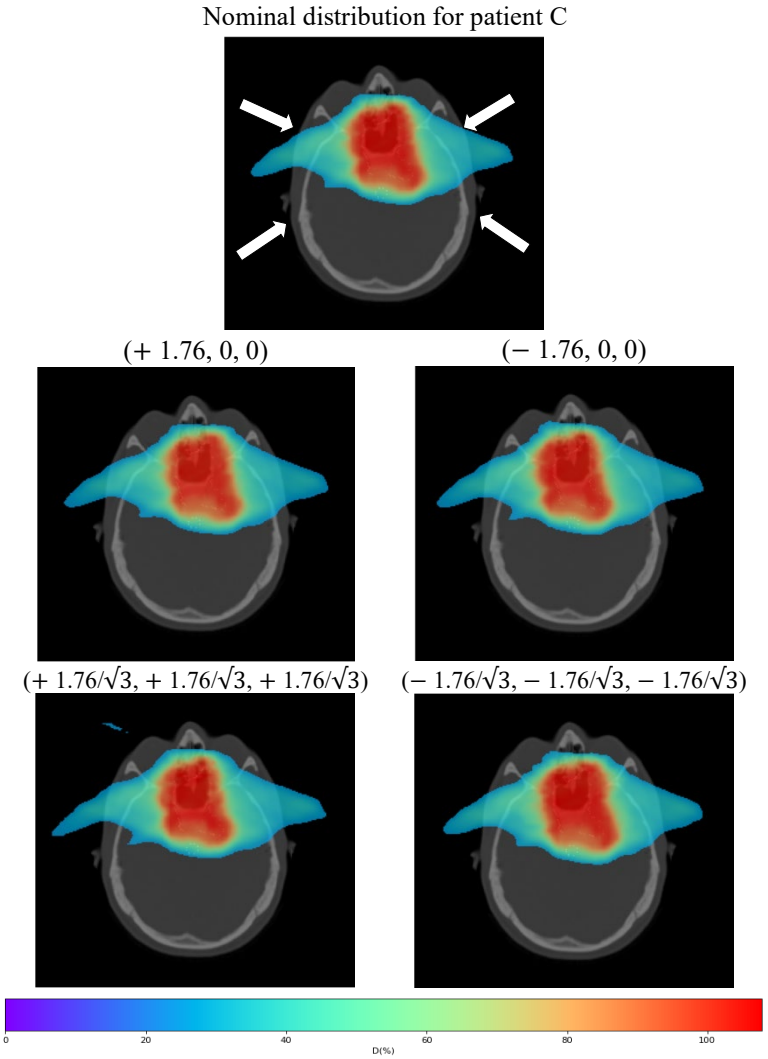

Figure 8: Axial slices for the third patient showing the nominal dose distribution (top), with arrows indicating the beam angles, and the resulting dose distributions for (± 1.76, 0, 0) (middle) and (±1.76/√3, ± 1.76/√3, ± 1.76/√3) (bottom) translations. The CTV and the brainstem are delineated. Dose bar shows the percentage dose relative to the prescribed dose to the target volume, shown on the same scale for all dose distributions.

4.2. DVH

In the following, quantitative information is obtained from the DVH curves generated from the dose distributions above, for the three patients in this study. The dose delivered to 95% of the volume of the CTV (D_{95}) and the dose that 2% of the volume of the OAR (D_2) receives are used to quantify the results. Dose is displayed as percentage dose relative to the prescribed dose to the target volume.

4.2.1. Patient 1

The regions of interest (ROI) relevant to display for the first patient are the CTV, the brainstem and the cerebellum. Figure 9 shows the DVH corresponding to the rotational errors and the DVH from figure 10 correspond to scalar shifts (see Appendix for additional rotations: (0º, ±1º, 0º), (±1º, 0º, 0º), (± 1º, ± 1º, ±1º) (figures 35, 36) and translations: (0, ± 1.76, 0), (0,0, ± 1.76), (±1.76/√3, ± 1.76/√3, ± 1.76/√3) (figures 37, 38)).

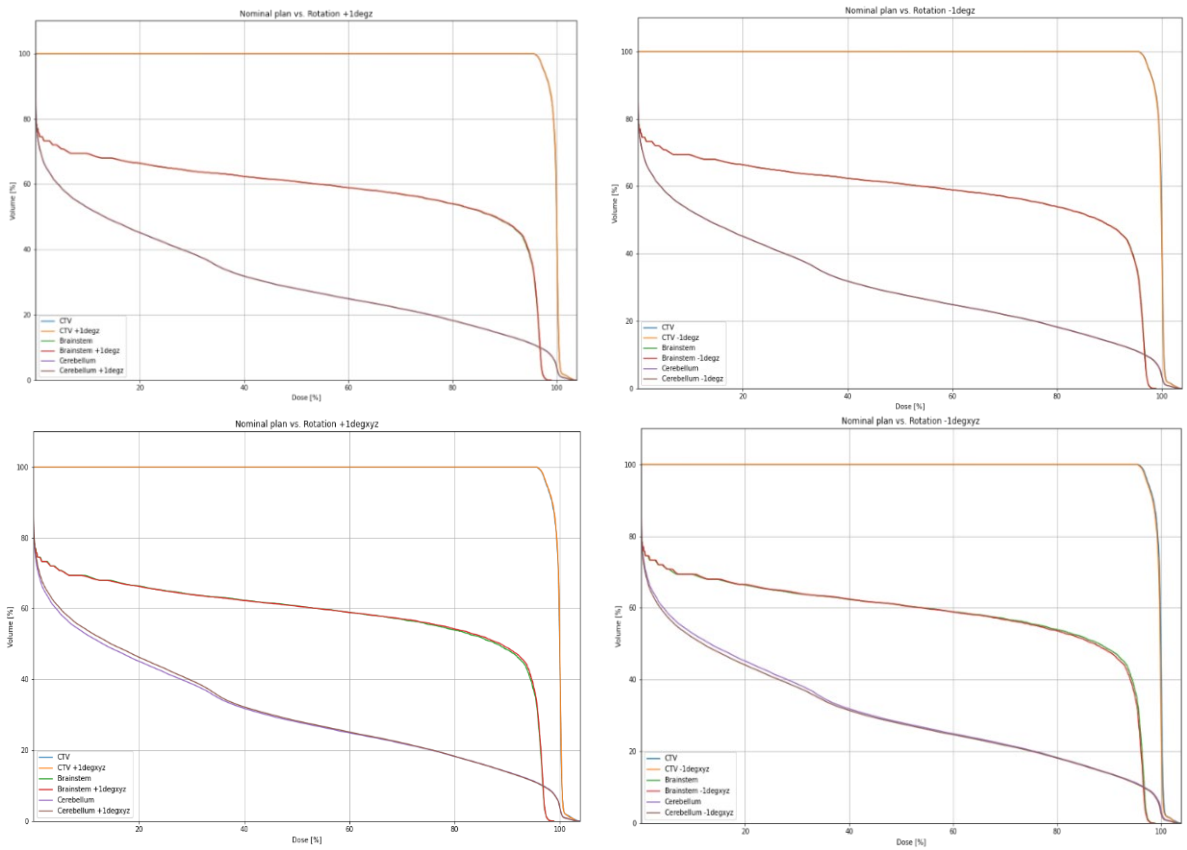

Figure 9: DVH for patient 1 in the case of (0º, 0º, ±1º) (top) and (± 1º, ± 1º, ±1º) (bottom) rotational errors vs. DVH for the nominal plan

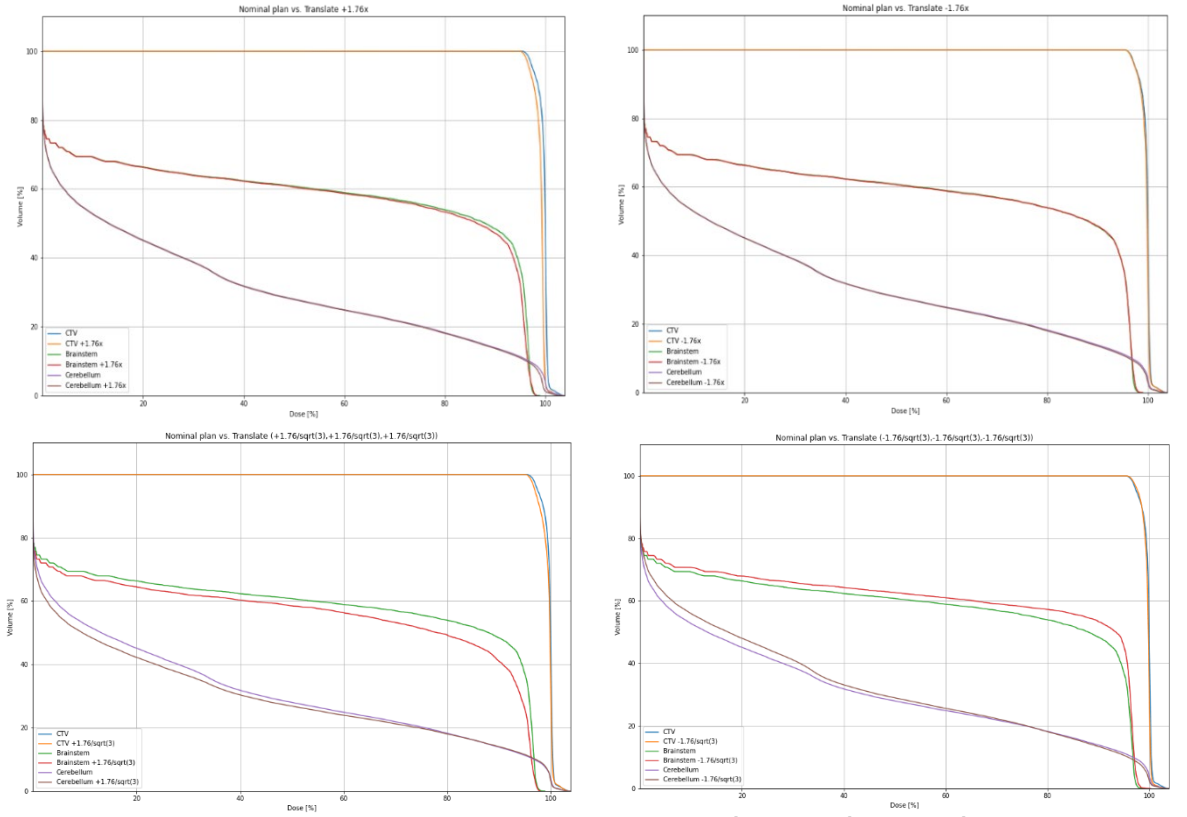

Figure 10: DVH for patient 1 in the case of (± 1.76, 0, 0) (top) and (±1.76/√3, ± 1.76/√3, ± 1.76/√3) (bottom) translations vs. DVH for the nominal plan

Regarding the dose delivered to the CTV, the DVH bands for the first patient indicate that, in the case of both rotational and translational errors, there seems to be good agreement with the nominal plan for all the selected directions. However, for the OAR, qualitatively, the plans corresponding to ($\pm 1.76/\sqrt{3}$, $\pm$ $1.76/\sqrt{3}$, $\pm$ $1.76/\sqrt{3}$) shifts exhibit higher sensitivity to delivery uncertainties (figure 10, bottom). This can be seen from the increase in width between the DVH bands for the nominal plan and the recalculated plan, compared to the case of rotational errors (figure 9) and ($\pm$ 1.76, 0, 0) translations (figure 10, top).

Quantitatively, when rotations are implemented, D_{95} and D_2 remain unchanged with respect to the nominal plan: 1.75 Gy_{RBE} (97.2%) for the CTV, 1.74 Gy_{RBE} (96.7%) for the brainstem and 1.81 Gy_{RBE} (101%) for the cerebellum. Regarding translations, there is only a marginal decrease in D_{95} below 1.74 Gy_{RBE} (96.6%) for the (+ 1.76, 0, 0) and ($+1.76/\sqrt{3}$,$+1.76/\sqrt{3}$, $+1.76/\sqrt{3}$) directions (figure 10, left) and a slight increase in D_2 for the brainstem above 1.75 Gy_{RBE} (96.7%) in the ($-1.76/\sqrt{3}$, $-$ $1.76/\sqrt{3}$, $-$ $1.76/\sqrt{3}$) direction (figure 10, bottom right). D_2 for the cerebellum remains the same, at 1.81 Gy_{RBE} (101%).

4.2.2. Patient 2

The regions of interest (ROI) relevant to display for the second patient are the CTV, the brainstem and the left eye. Figure 11 is representative of the DVH for rotational setup errors and figure 12 shows the DVH for translational uncertainties (see Appendix for additional rotations: (0º, $\pm$1º, 0º), ($\pm$1º, 0º, 0º), ($\pm$ 1º, $\pm$ 1º, $\pm$1º) (figures 39, 40) and translations: (0,$\pm$1.76, 0), (0, 0, $\pm$ 1.76), ($\pm 1.76/\sqrt{3}$, $\pm$ $1.76/\sqrt{3}$, $\pm$ $1.76/\sqrt{3}$) (figures 41, 42)).

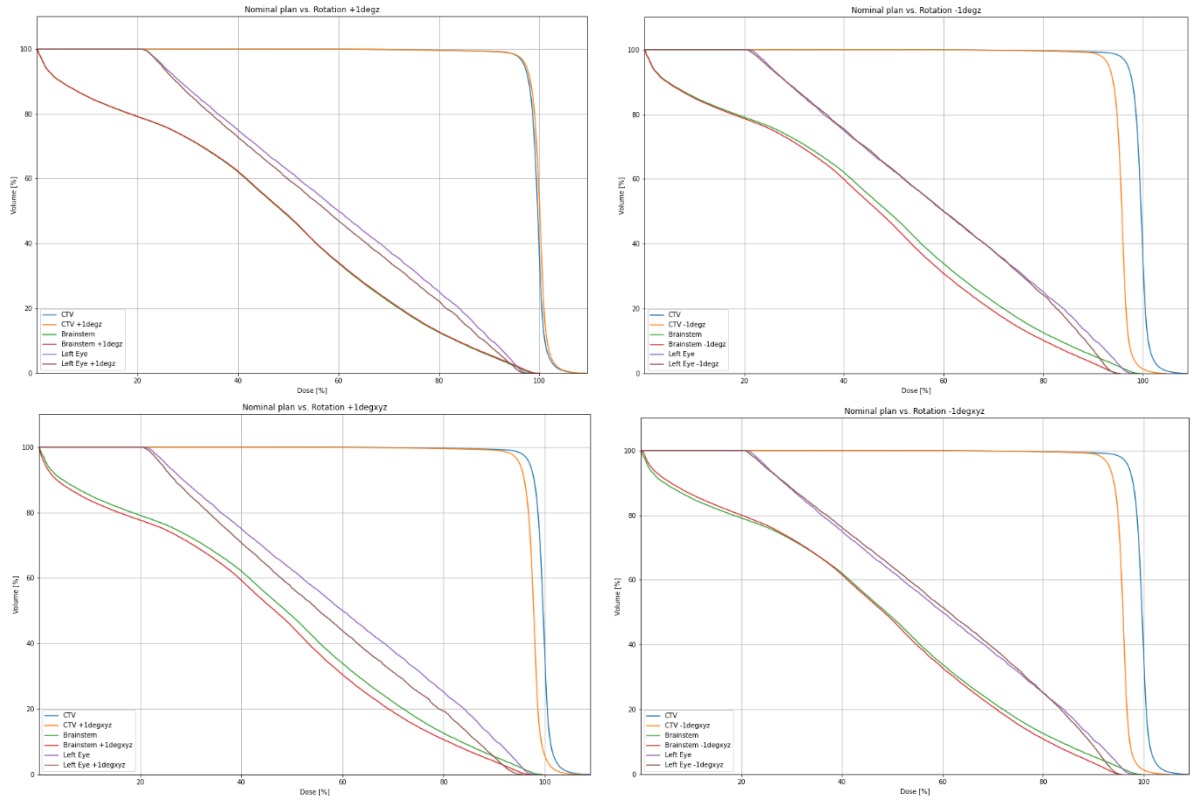

Figure 11: DVH for patient 2 in the case of (0º, 0º, $\pm$1º) (top) and ($\pm$ 1º, $\pm$ 1º, $\pm$1º) (bottom) rotational errors vs. DVH for the nominal plan

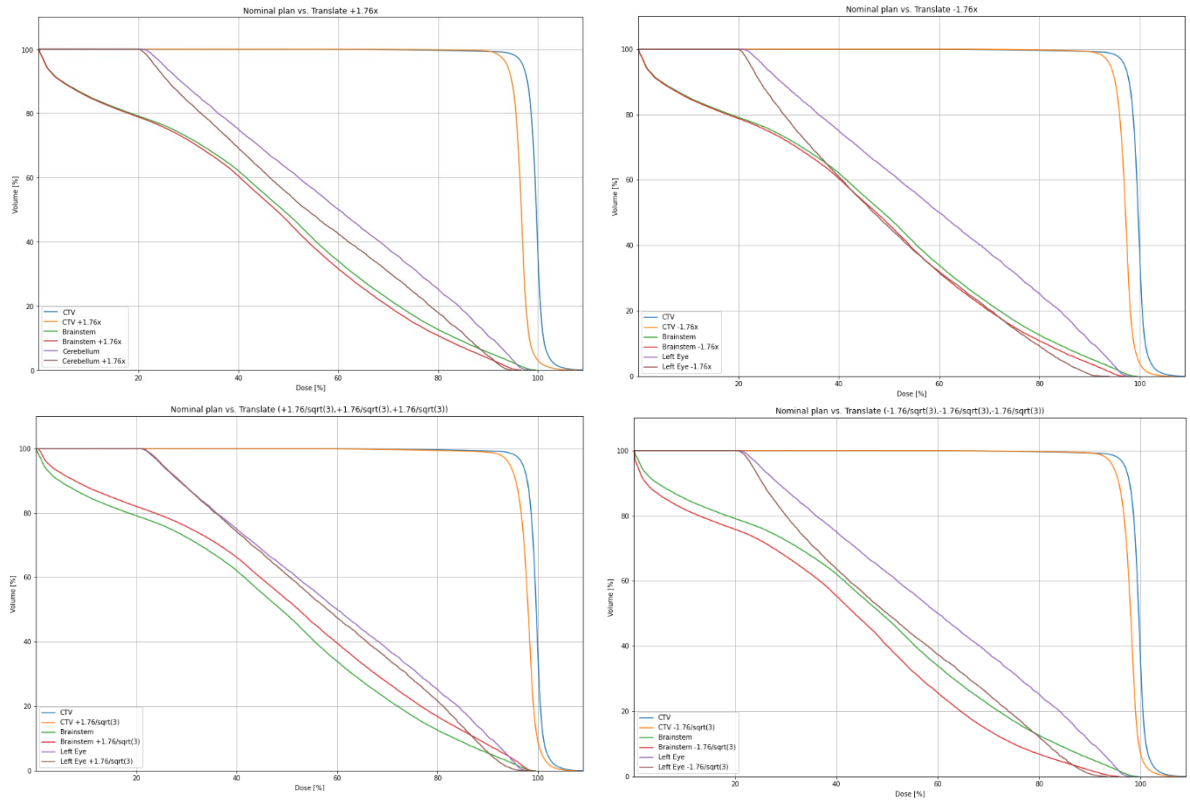

Figure 12: DVH for patient 2 in the case of ($\pm$ 1.76, 0, 0) (top) and ($\pm 1.76/\sqrt{3}$, $\pm 1.76/\sqrt{3}$, $\pm 1.76/\sqrt{3}$) (bottom) translations vs. DVH for the nominal plan

Upon visual inspection, in terms of sparing the OAR, the DVH bands corresponding to the selected directions of rotation indicate that there is overall good agreement with the nominal plan (figure 11). In the case of patient shifts, between the nominal plan and the recalculated plan, wider DVH bands are visible in this case as well, especially noticeable in the negative direction, corresponding to the left eye (figure 12, right). For the CTV, larger DVH bands are seen for the (0,0, -1^{o}) and (-1^{o},-1^{o}, -1^{o}) rotations (figure 11, right) compared to the opposite directions of rotation (figure 11, left). When translations are simulated, the DVH bands for the CTV appear to have the same width (figure 12).

Quantitatively, D_2 for the brainstem decreases from 1.78 Gy_{RBE} (97.5%) (corresponding to D_2 for the nominal plan) to approximately 1.71 Gy_{RBE} (94%) for both uncertainty scenarios, with a few exceptions: D_2 remains unchanged for the (0, 0, $+1^{o}$) rotation (figure 11, top left) and increases slightly above 1.78 Gy_{RBE} (97%) in the ($+1.76/\sqrt{3}$, $+1.76/\sqrt{3}$, $+1.76/\sqrt{3}$) direction. For the left eye, there is a reduction in D_2 below the value of the nominal plan, 1.76 Gy_{RBE} (96.4%), in both error scenarios. This is more noticeable in the (-1.76, 0, 0) and ($-1.76/\sqrt{3}$, $-1.76/\sqrt{3}$, $-1.76/\sqrt{3}$) directions (figure 12, right), where D_2 decreases to 1.62 Gy_{RBE} (89%). Regarding the CTV, (0,0, -1^{o}) and (-1^{o},-1^{o}, -1^{o}) rotations have more impact on D_{95}, which decreases from 1.77 Gy_{RBE} (97%) to 1.68 Gy_{RBE} (92%) (figure 11, right) and reduces to 1.73 Gy_{RBE} (95%) in the case of translations (figure 12). Such variations, both in the case of the CTV and in terms of sparing the OAR, were not as obvious from the dose distributions (figures 5, 6) and may be due to the complex shape of the target volume.

4.2.3. Patient 3

The regions of interest (ROI) relevant to display for the third patient are the CTV, the brainstem and the left eye. The effects of positioning uncertainties can be visualised in figure 13 for the rotations and in figure 14 for the rigid translations (see Appendix for additional

rotations: (0º, ±1º, 0º), (±1º, 0º, 0º), (± 1º, ± 1º, ±1º) (figures 43, 44) and translations: (0,±1.76, 0), (0, 0, ± 1.76), (±1.76/√3, ± 1.76/√3, ± 1.76/√3) (figures 45, 46)).

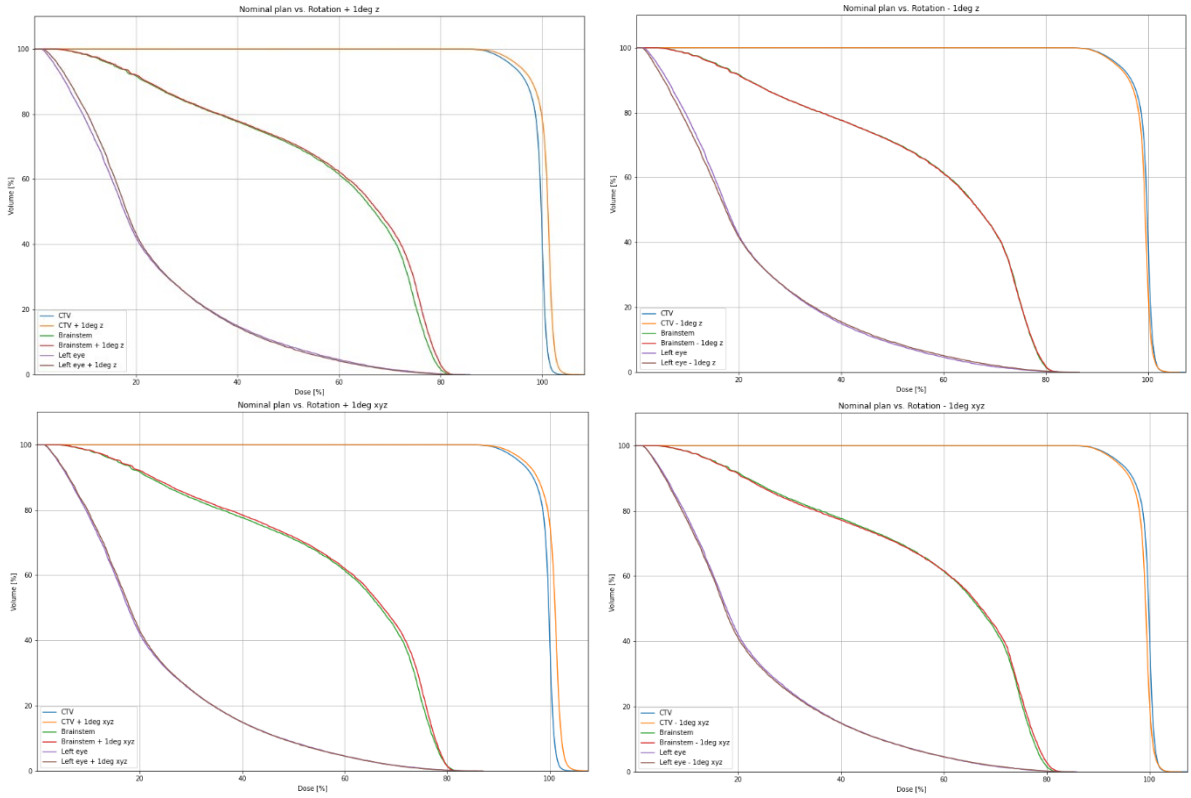

Figure 13: DVH for patient 3 in the case of (0º, 0º, ±1º) (top) and (± 1º, ± 1º, ±1º) (bottom) rotational errors vs. DVH for the nominal plan

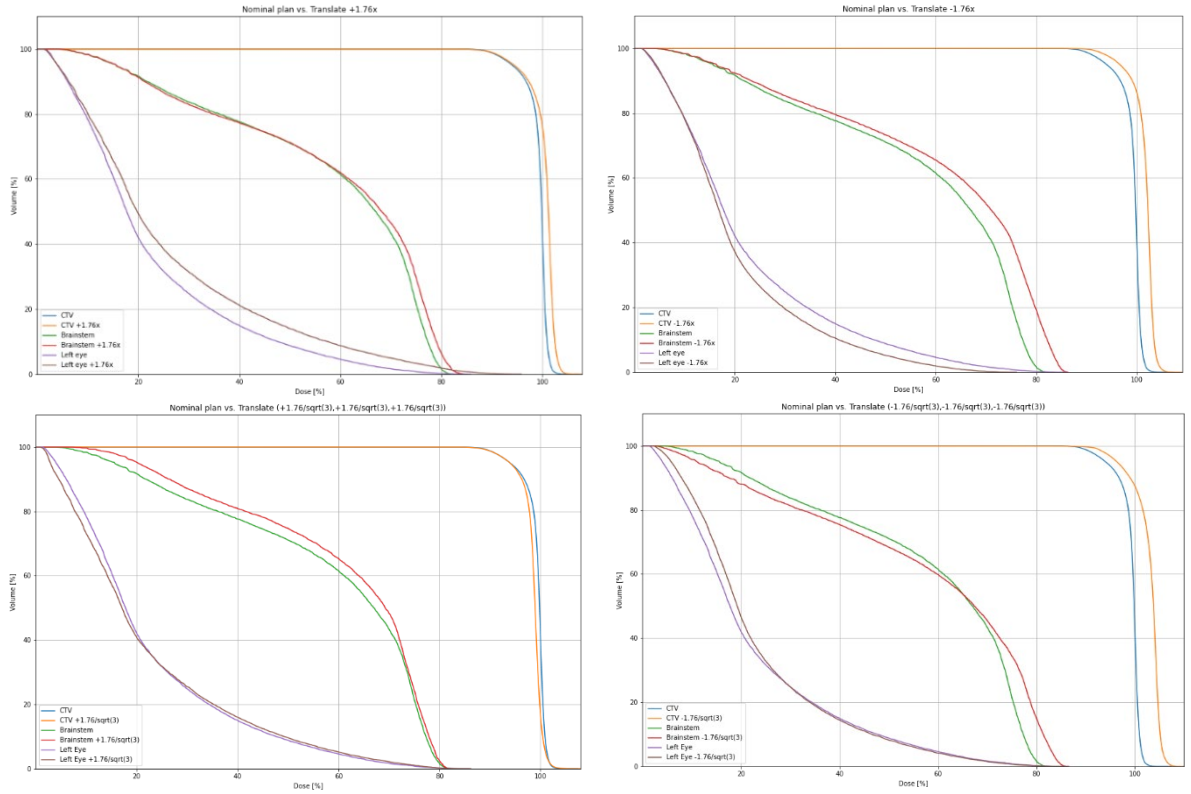

Figure 14: DVH for patient 3 in the case of (± 1.76, 0, 0) (top) and (±1.76/√3, ± 1.76/√3, ± 1.76/√3) (bottom) translations vs. DVH for the nominal plan

Qualitatively, the DVH bands for the third patient show that rotations (figure 13) have very little impact on the delivered dose compared to that of scalar shifts, as can be observed from the width of the DVH bands between the nominal plan and the recalculated plan for each ROI. This is also valid for the (+ 1.76, 0, 0) and (+1.76/√3, +1.76/√3, +1.76/√3) translations.

The effect of displacements is more proeminent on the brainstem, as the DVH band shows an increase in D_2 from 1.61 Gy_{RBE} (79%) (corresponding to the nominal plan) to 1.69 Gy_{RBE} (83%) for negative shifts (figure 14, right). They also lead to an overshoot of the CTV, as D_{95} increases from 1.9 Gy_{RBE} (94%) to 1.92 Gy_{RBE} (95%). D_2 to the left eye increases from 1.45 Gy_{RBE} (71%) to 1.67 Gy_{RBE} (82%) for the (+ 1.76, 0, 0) shift and decreases to 1.26 Gy_{RBE} (62%) for the (− 1.76, 0, 0) shift (figure 14, top).

4.3. Worst – case distribution

The simulated lower and upper bounds on the plan quality are displayed separately for the ROI corresponding to each patient, using the combined distributions for the error scenarios in the case of rotations and translations.

The results for the three patients are shown below (figures 15 – 20). For visualisation purposes, CTV relative doses between 80% - 100% of the prescription dose are displayed [7]. Similar to the quantitative analysis of the DVH in section 4.2, D_{95} and D_2 will be evaluated, corresponding to the dose to the CTV and the brainstem, respectively.

4.3.1. CTV

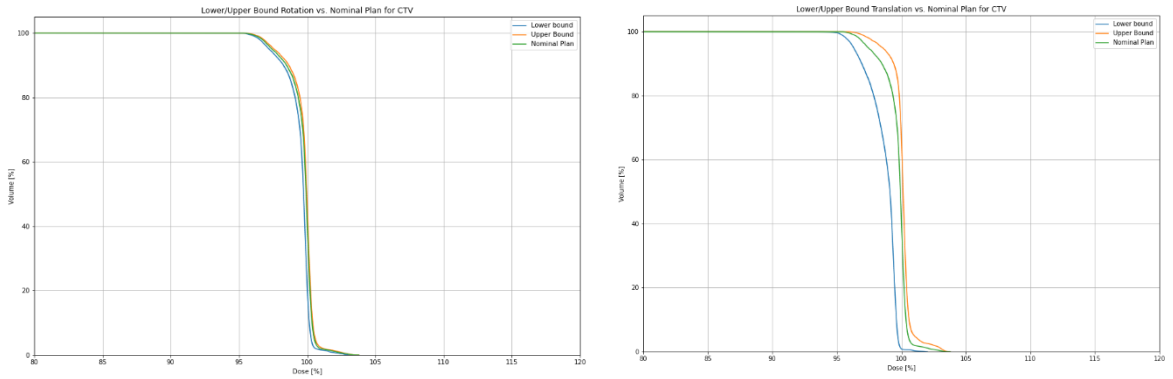

Figure 15: Patient 1 - DVH for the CTV showing the lower and upper bound on the treatment plan quality: rotational uncertainties (left) and translational uncertainties (right)

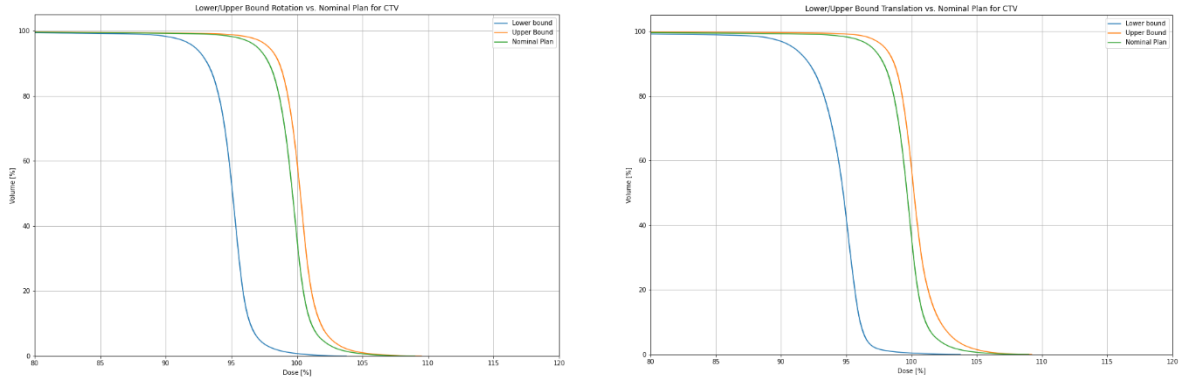

Figure 16: Patient 2 - DVH for the CTV showing the lower and upper bound on the treatment plan quality: rotational uncertainties (left) and translational uncertainties (right)

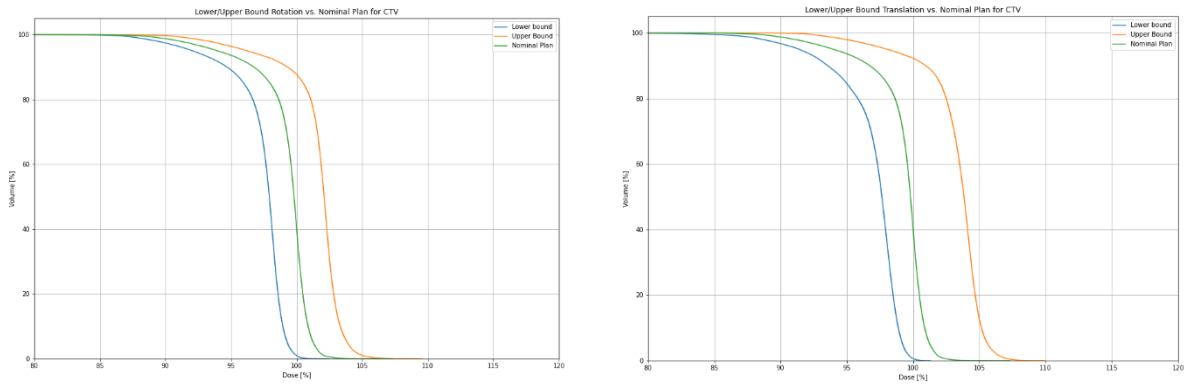

Figure 17: Patient 3 - DVH for the CTV showing the lower and upper bound on the treatment plan quality: rotational uncertainties (left) and translational uncertainties (right)

Graphical analysis shows that the DVH of the nominal plan is located between the uncertainty levels corresponding to the DVH bands of the simulated upper and lower bounds. This is valid for all three patients (figures 15 – 17). When rotational errors are implemented, it appears that the bounds of the plan are brought closer together compared to the translational error scenario.

Rotational uncertainties indicate that the range between the lower and upper bounds is smallest for the first patient, showing good agreement with the nominal plan, where D_{95} is 1.75 Gy_{RBE} (97.2%). Translational errors lead to a larger difference between the bounds on the plan quality, as D_{95} corresponding to the worst – case DVH band is 1.72 Gy_{RBE} (96%) and increases to 1.78 Gy_{RBE} (99%) for the best – case DVH band. The values of D_{95} are shown in table 2 for all patients.

Table 2: D_{95} values for the CTV in the case of rotational and translational setup uncertainties

	CTV D_{95} (Gy_{RBE})					
	Rotational positioning uncertainties			Translational setup uncertainties		
Cases	Worst – case	Nominal plan	Best – case	Worst – case	Nominal plan	Best – case
1		97.2% (1.75)		96% (1.72)	97.2% (1.75)	99% (1.78)
2	92.5% (1.68)	97% (1.77)	98% (1.78)	91.5% (1.67)	97% (1.77)	98% (1.78)
3	92% (1.86)	94% (1.9)	96% (1.94)	91.7% (1.85)	94% (1.9)	97.5% (1.97)

Using the values from table 2, the percentage difference between the values of D_{95} corresponding to the worst – case and best – case scenarios for the CTV can be computed for each patient. As a result, rotational errors yield only a marginal difference for the first patient, 5.5% difference for the second patient and 4% for the third patient. By contrast, translational setup errors lead to a 3% difference for the first patient, 6.5% for the second patient and 5.8% for the third patient.

4.3.2. OAR

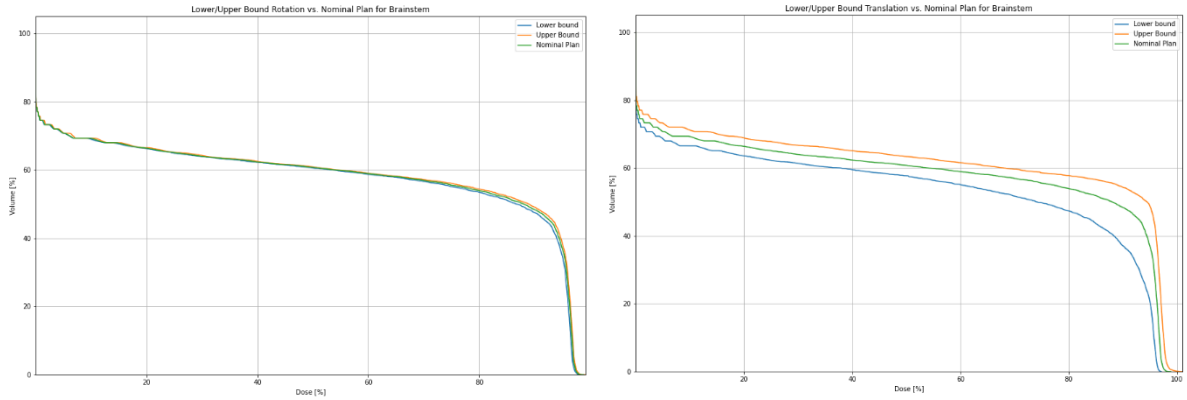

Figure 18: Patient 1 - DVH for the brainstem showing the lower and upper bound on the treatment plan quality: rotational uncertainties (left) and translational uncertainties (right)

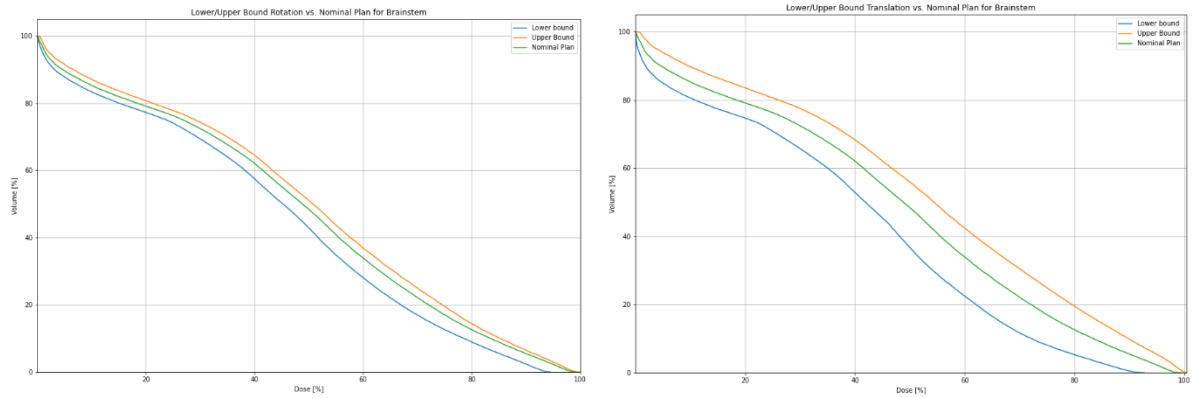

Figure 19: Patient 2 - DVH for the brainstem showing the lower and upper bound on the treatment plan quality: rotational uncertainties (left) and translational uncertainties (right)

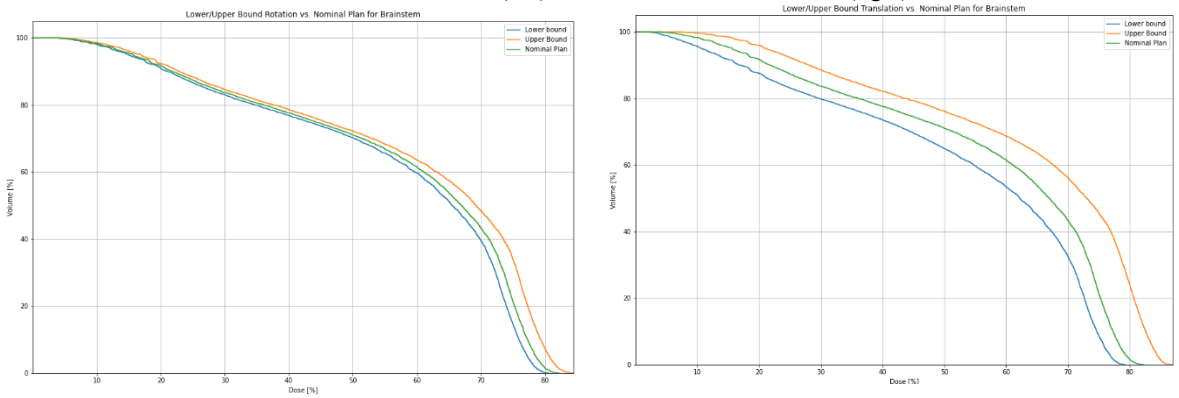

Figure 20: Patient 3 - DVH for the brainstem showing the lower and upper bound on the treatment plan quality: rotational uncertainties (left) and translational uncertainties (right)

Similar to the findings in section 4.3.1, the DVH for the brainstem in figures 18 – 20 show a smaller difference between the simulated bounds corresponding to the rotational uncertainties. This is also valid for all three patients.

Quantitatively, similar to D_{95}, the interval between the bounds on the plan quality, when rotations are implemented, is smallest for the first patient, showing good agreement with the nominal plan, where D_2 is 1.74 Gy_{RBE} (96.7%). In the case of translational uncertainties, D_2 corresponding to the lower bound is 1.72 Gy_{RBE} (95.5%) and increases to 1.76 Gy_{RBE} (98%). The values of D_2 are shown in table 3 for all patients (see Appendix for DVH for the cerebellum of the first patient (figure 47, table 6) and left eye in the case of the second and third patient (figures 48 – 49, table 7)).

Table 3: D_2 values for the brainstem in the case of rotational and translational setup uncertainties

	Brainstem D_2 (Gy_{RBE})					
	Rotational positioning uncertainties			Translational setup uncertainties		
Cases	Best – case	Nominal plan	Worst – case	Best – case	Nominal plan	Worst – case
1		96.7% (1.74)		95.5% (1.72)	96.7% (1.74)	98% (1.76)
2	91% (1.66)	97.5% (1.78)	98% (1.79)	88.5% (1.61)	97.5% (1.78)	99% (1.8)
3	78% (1.59)	79% (1.61)	82% (1.67)	76.5% (1.56)	79% (1.61)	83.5% (1.7)

Similar to the section 4.3.1, the percentage difference between the values of D_2 corresponding to the worst – case and best – case scenarios for the brainstem can be computed for each patient: there is only a marginal difference for the first patient, 7% for the second patient and 4% for the third patient. However, for translational setup errors, there is a 2.5% difference for the first patient, 10.5% for the second patient and 7% for the third patient.

4.4. Error bar distributions and EVH

Using equation (1), error bars have been calculated separately for the 14 error scenarios in the case of rotational deviations and 14 error scenarios for the scalar shifts, while also taking into account the nominal plan. Figure 21 shows the normalised error bar distributions for the three patients, such that the percentage dose differences are relative to the prescribed dose to the target volume.

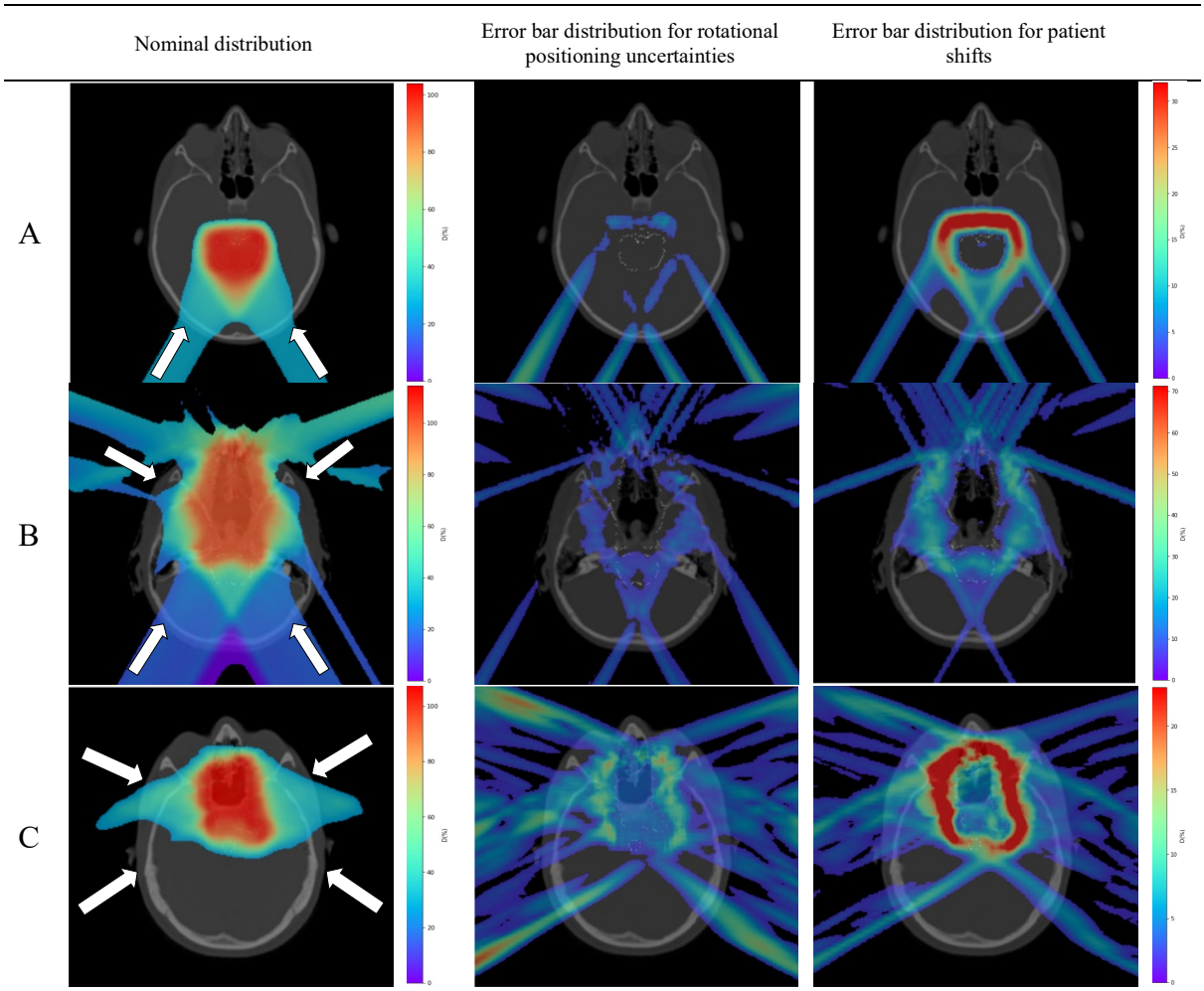

Figure 21: Axial slices for the three patients showing the nominal dose distributions (left), with arrows indicating the beam angles, and the error bar distributions corresponding to the rotational errors (middle) and translational shifts (right). The CTV and the brainstem are delineated. The percentage dose differences are relative to the prescribed dose to the target volume. The error bar dose distributions for each patient, in both uncertainty conditions, are scaled the same for comparison.

From figure 21, the error bar distributions exhibit a relatively robust dose to the CTV in both uncertainty conditions, with small variations in favour of the rotational errors, while for the brainstem the larger error bars correspond to the plan affected by translational shifts of the patient.

Robustness is assessed by extracting the EVH from the error bar distributions for the delineated ROI, which can provide more information. $E_{2\%}$ is used as metric for the error bar to 2% of the selected delineated structures. Figure 22 is representative of the EVH for the CTV and the brainstem, analysed for each patient.

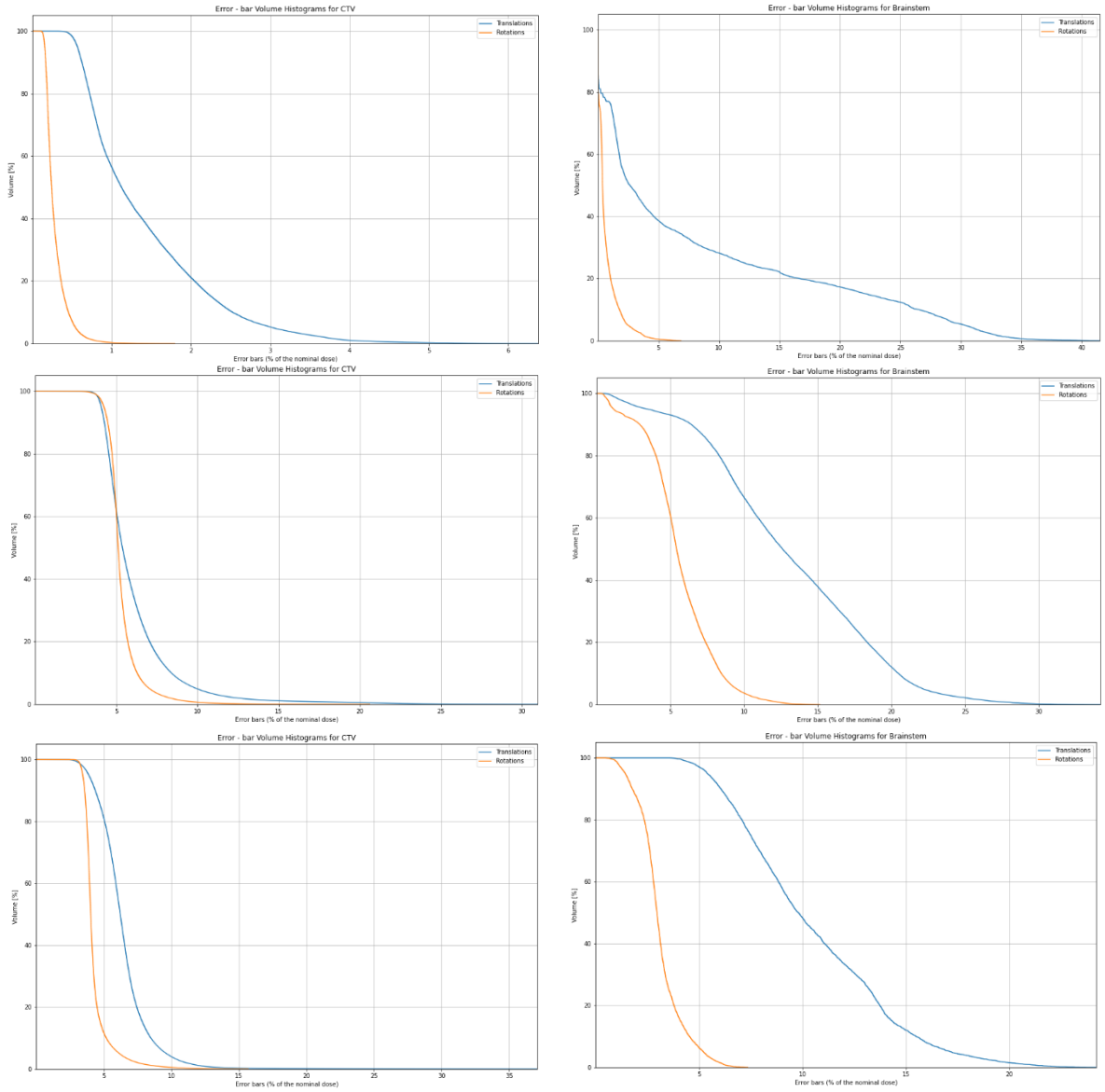

Figure 22: Error bar volume histograms for the CTV (left) and brainstem (right), for the first (top), second (middle) and third (bottom) patient, representative of the rotational (in orange) and translational (in blue) setup errors

Graphically, under the rotational error scenario, figure 22 shows that the dose to the CTV is more robust dose than in the case of scalar shifts, as the EVH curve is shifted more to the bottom – left corner. Quantitatively, for the first patient (figure 22, top left), 2% of the CTV has an error bar magnitude of more than 0.7% ($E_{2\%} > 0.7\%$) for rotational setup errors and more than 3.7% ($E_{2\%} > 3.7\%$) in the case of rigid displacements. The results for the patients are shown in table 4.

Table 4: Error bar values for the CTV in the case of rotational and translational setup uncertainties

	CTV $E_{2\%}$	
Cases	Rotational positioning uncertainties	Translational setup uncertainties
1	> 0.7%	> 3.7%
2	> 10%	> 16%
3	> 7.5%	> 12%

This is valid for the brainstem as well, indicating that rotational uncertainties have considerably less impact on the treatment and OAR sparing is maintained. Looking at the magnitudes, for the first patient (figure 22, top right), 2% of the brainstem has an error bar magnitude of more than 4% ($E_{2\%} > 4\%$) for rotational setup errors. However, in the case of translations, the minimum magnitude is 33% ($E_{2\%} > 33\%$), which emphasizes the high sensitivity of the OAR to patient shifts. The results for the patients are shown in table 5 (see Appendix for the error bar values corresponding to the cerebellum (first patient) (figure 50, table 8) and the left eye (second and third patient) (figure 51, table 9)).

Table 5: Error bar values for the brainstem in the case of rotational and translational setup uncertainties

	Brainstem $E_{2\%}$	
Cases	Rotational positioning uncertainties	Translational setup uncertainties
1	> 4%	> 33%
2	> 12%	> 27.5%
3	> 5.5%	> 12%

5. Conclusion and discussion

In summary, in this project the methodological aspects of proton treatment robustness have been addressed, providing a toolbox for simulating six degree – of – freedom setup uncertainties. The followed approach, namely manipulating the planning CT images, is generally applicable and does not require changes in the treatment planning system. This method has been used to evaluate the robustness of three head and neck cases from the database of delivered plans. Dose distributions were recalculated for a total of 14 rotational error scenarios and 14 translational ones, implemented for each patient. Dose–volume histograms, error bar distributions and error bar volume histograms were then used to assess plan robustness.

The dose distributions from figures 3 – 8 showed that, despite delivery uncertainties, dose homogeneity and coverage of the CTV were only marginally affected. However, it is known that dose distributions are difficult to evaluate visually as there is a large amount of information to assess. As a result, dose–volume histograms were extracted for the three patients to investigate the sensitivity of the recalculated plans to setup errors (figures 9 – 14) and D_{95} for the CTV together with D_2 for the OAR were assessed. For the second patient, degradation of the plan quality was present in both uncertainty conditions (figures 11,12). This may be due to the more complex shape of the target volume and beam arrangement with fields crossing a

larger area of variable density. Dose delivery remained robust in the case of rotational errors for the first and third patient, showing good agreement with the nominal plan (figures 9, 13).

Furthermore, evaluation of the worst – case distribution for the CTV (figures 15 – 17) and OAR (figures 18 – 20) was performed. Values for D_{95} and D_2 were tabulated for the lower and upper bounds on the plan quality (tables 2 and 3). However, the worst – case analysis is not a reliable method to use when assessing robustness, due to the assumption that voxels are not correlated [13]. Given this, an error bar evaluation is more appropriate.

Error bar distributions (figure 21) and the corresponding error bar volume histograms (figure 22) lead to a quantitative analysis of the robustness of proton plans. Treatment plans prove to be more robust against rotational positioning uncertainties than translations, validated by EVH bands and smaller error bar magnitudes (tables 2 and 3): $E_{2\%} > 0.7\%$ (rotations), $E_{2\%} > 3.7\%$ (translations) for the CTV and $E_{2\%} > 4\%$ (rotations), $E_{2\%} > 33\%$ (translations) for the brainstem of the first patient.

Rotational and translational positioning uncertainties were evaluated separately and range uncertainties were not taken into account. The translations which were implemented were based on experiments conducted at PSI. However, for rotational setup errors, no data has been recorded at PSI, but reasonable assumptions were made in this study when using a magnitude of 1º. Future work can include larger magnitudes of rotation to study their effects on proton treatment plans. Moreover, robustness analysis which includes a combination of the two setup error scenarios and also the impact of different ranges of the proton beam is of interest. The latter is especially interesting for head and neck cases, where the anatomy is complex and the fillings of the nasal cavity can vary.

Experimental – based methods could extend our work through phantom measurements, precisely translating and rotating it using a positioning jig in order to validate the dose discrepancies. Moreover, given that this study was performed based on a single dose fraction delivery, as we move towards a fractionation scheme, we can expect better results in terms of proton plan robustness to uncertainties [7].

References

[1] Albertini F., Hug E. B., Lomax A. 2011 Is it necessary to plan with safety margins for actively scanned proton therapy? *Phys. Med. Biol* **56**, 4399 - 4413. (doi: 10.1088/0031-9155/56/14/011)

[2] Lomax A. 1999 Intensity modulation methods for proton radiotherapy. *Phys. Med. Biol.* **44***, 185 – 205* (doi: 10.1088/0031-9155/44/1/014)

[3] Fattori G., Riboldi M., Scifoni E., Krämer M., Pella A., Durante M., Ronchi S., Bonora M., Orecchia R., Baroni G. 2014 Dosimetric effects of residual uncertainties in carbon ion treatment of head chordoma. *Radiotherapy and Oncology* **113***,* 66 – 71 (https://doi.org/10.1016/j.radonc.2014.08.001)

[4] Chen W., Unkelbach J., Trofimov A., Madden T., Kooy H., Bortfeld T., Craft D. 2012 Including robustness in multi – criteria optimization for intensity – modulated proton therapy. *Phys. Med. Biol.* **57**, 591 – 608 (doi: 10.1088/0031-9155/57/3/591)

[5] Schaffner B., Pedroni E., Lomax A. 1999 Dose calculation models for proton treatment planning using a dynamic beam delivery system: an attempt to include density heterogeneity effects in the analytical dose calculation. *Phys. Med. Biol*. **44**, 27 – 41 (doi: 10.1088/0031-9155/44/1/004)

[6] Meyer J., Bluett J., Amos R., Levy L., Choi S., Nguyen Q. – N., Zhu R. Z., Gillin M., Lee A. 2010 Spot scanning proton beam therapy for prostate cancer: treatment planning technique and analysis of consequences of rotational and translational alignment errors. *Int. J. Radiation Oncology Biol. Phys.* **78**, 428 – 434 (doi: 10.1016/j.ijrobp.2009.07.1696)

[7] Lowe M., Albertini F., Aitkenhead A., Lomax A., MacKay R. 2016 Incorporating the effect of fractionation in the evaluation of proton plan robustness to setup errors. *Phys. Med. Biol.* **61**, 413 – 429 (doi: 10.1088/0031-9155/61/1/413)

[8] Schneider U., Pedroni E., Lomax A. 1996 The calibration of CT Hounsfield units for radiotherapy treatment planning. *Phys. Med. Biol.* **41**, 111 – 124 (doi: 10.1088/0031-9155/41/1/009)

[9] Unkelbach J., Bortfeld T., Martin B. C., Soukup M. 2009 Reducing the sensitivity of IMPT treatment plans to setup errors and range uncertainties via probabilistic treatment planning. *Med. Phys*. **36** (doi: 10.1118/1.3021139)

[10] Bolsi A., Lomax A., Pedroni E., Goitein G., Hug E. 2008 Experiences at the Paul Scherrer Institute with a remote patient positioning procedure for high – throughput proton radiation therapy. *Int. J. Radiation Oncology Biol. Phys.* **71**, 1581 – 1590 (https://doi.org/10.1016/j.ijrobp.2008.02.079)

[11] Goitein M. 1985 Calculation of the uncertainty in the dose delivered during radiation therapy. *Med. Phys.* **12**, 608 – 612 (https://doi.org/10.1118/1.595762)

[12] Lomax A. *et al* 2001 Intensity modulated proton therapy: a clinical example. *Med. Phys.* **28**, 317 – 324 (doi: 10.1118/1.1350587)

[13] Pflugfelder D., Wilkens J. J., Oelfke U. 2008 Worst case optimization: a method to account for uncertainties in the optimization of intensity modulated proton therapy. *Phys. Med. Biol.* **53**, 1689 – 1700 (doi: 10.1088/0031-9155/53/6/013)

[14] Casiraghi M., Albertini F., Lomax A. 2013 Advantages and limitations of the "worst case scenario" approach in IMPT treatment planning. *Phys. Med. Biol.* **58**, 1323 – 1339 (doi: 10.1088/0031-9155/58/5/1323)

[15] Goitein M. 1983 Nonstandard deviations. *Med. Phys.* **10**, 709 – 711 (doi: 10.1118/1.595409)

[16] Trofimov A., Unkelbach J., DeLaney T. F., Bortfeld T. 2011 Visualisation of a variety of possible dosimetric outcomes in radiation therapy using dose – volume histogram bands. *Practical Radiation Oncology* **2**, 164 – 171 (https://doi.org/10.1016/j.prro.2011.08.001)

[17] Lomax A., 2008 Intensity modulated proton therapy and its sensitivity to treatment uncertainties 2: the potential effects of inter – fraction and inter – field motions. *Phys. Med. Biol.* **53**, 1043 – 1056 (doi: 10.1088/0031-9155/53/4/015)

Appendix

A. Dose distributions

A.1. Patient A

A.1.1. Rotational setup errors

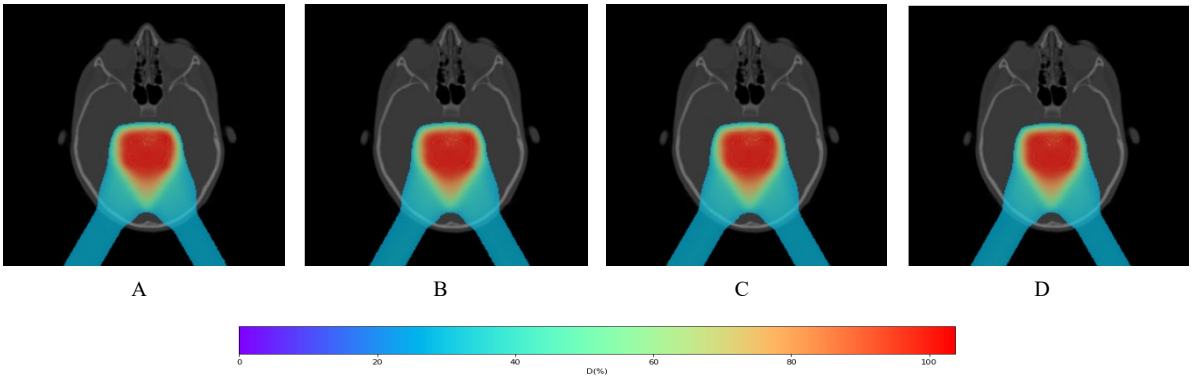

Figure 23: Rotational setup errors for (±1º, 0º, 0º) – A, B; (0º, ±1º, 0º) – C, D;

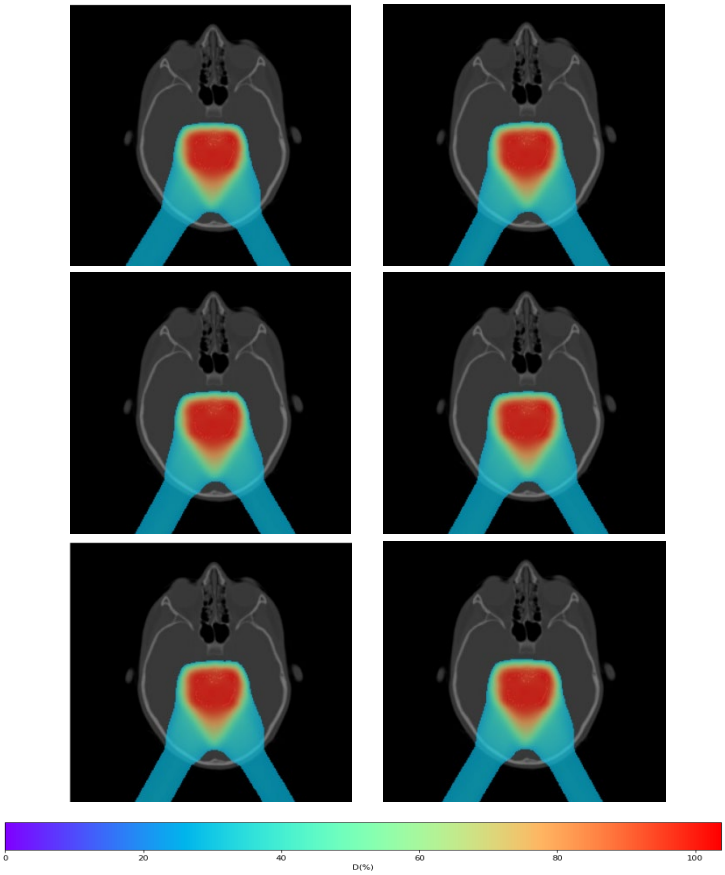

Figure 24: Rotational errors for (+ 1º, + 1º, −1º), (− 1º, − 1º, +1º) (top); (− 1º, + 1º, +1º), (+ 1º, − 1º, −1º) (middle); (+ 1º, − 1º, +1º), (− 1º, + 1º, −1º) (bottom)

A.1.2. Translational shifts

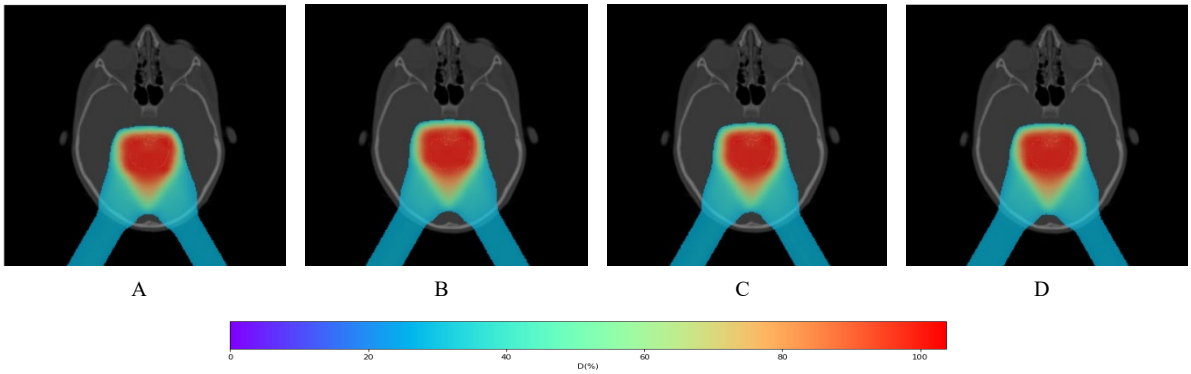

Figure 25: Translational setup errors for (0, ± 1.76, 0) – A, B; (0, 0, ± 1.76) – C, D

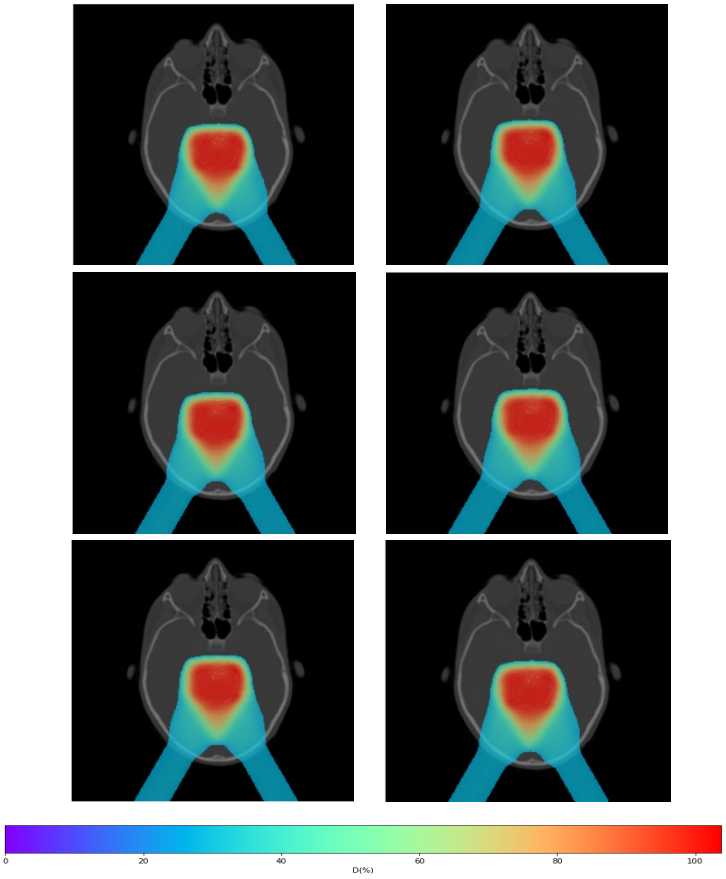

Figure 26: Translational errors for (+ 1.76/√3, + 1.76/√3, −1.76/√3), (− 1.76/√3, − 1.76/√3, +1.76/√3) (top); (− 1.76/√3, + 1.76/√3, +1.76/√3), (+ 1.76/√3, − 1.76/√3, −1.76/√3) (middle); (+ 1.76/√3, − 1.76/√3, +1.76/√3), (− 1.76/√3, + 1.76/√3, −1.76/√3) (bottom)

A.2. Patient B

A.2.1. Rotational setup errors

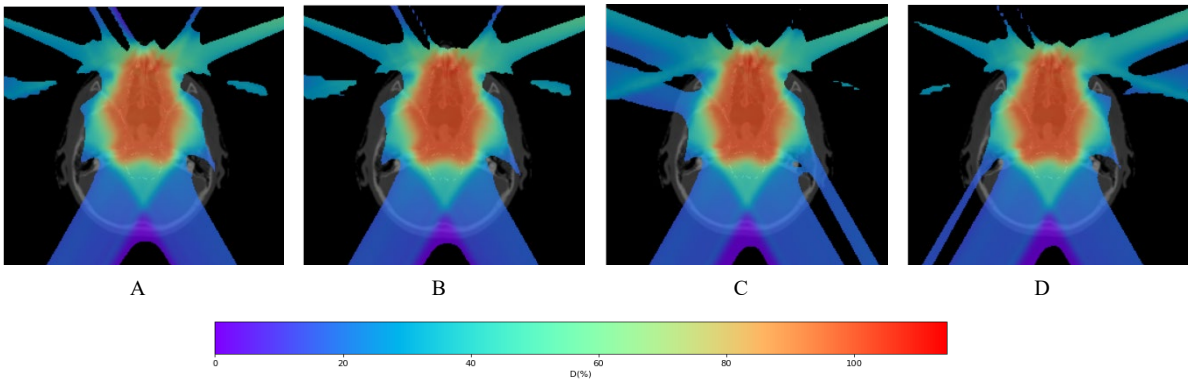

Figure 27: Rotational setup errors for (±1º, 0º, 0º) – A, B; (0º, ±1º, 0º) – C, D;

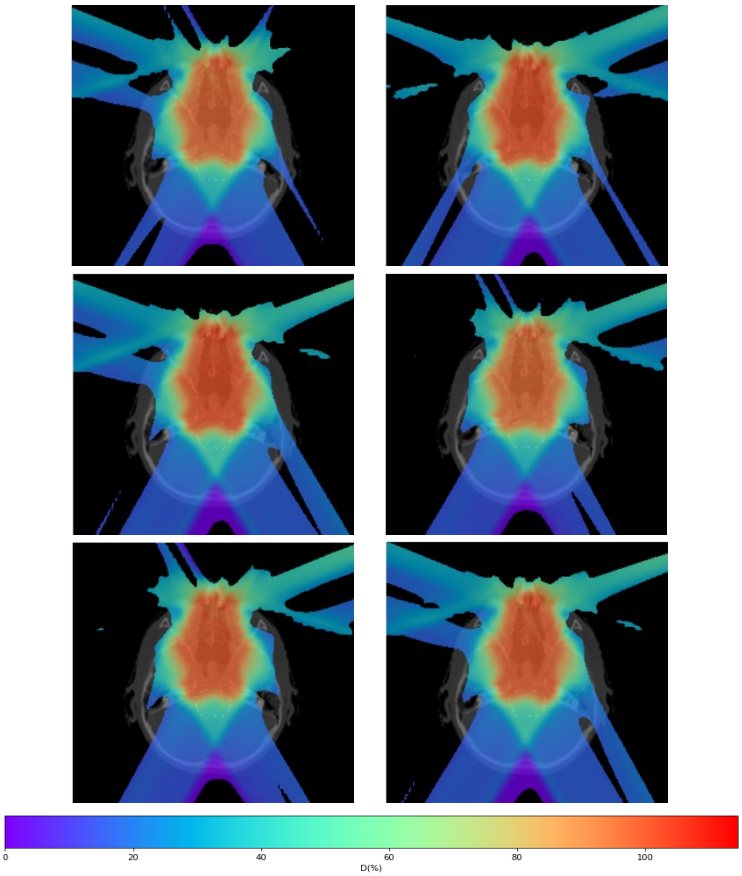

Figure 28: Rotational errors for (+ 1º, + 1º, −1º), (− 1º, − 1º, +1º) (top); (− 1º, + 1º, +1º), (+ 1º, − 1º, −1º) (middle); (+ 1º, − 1º, +1º), (− 1º, + 1º, −1º) (bottom)

A.2.2. Translational shifts

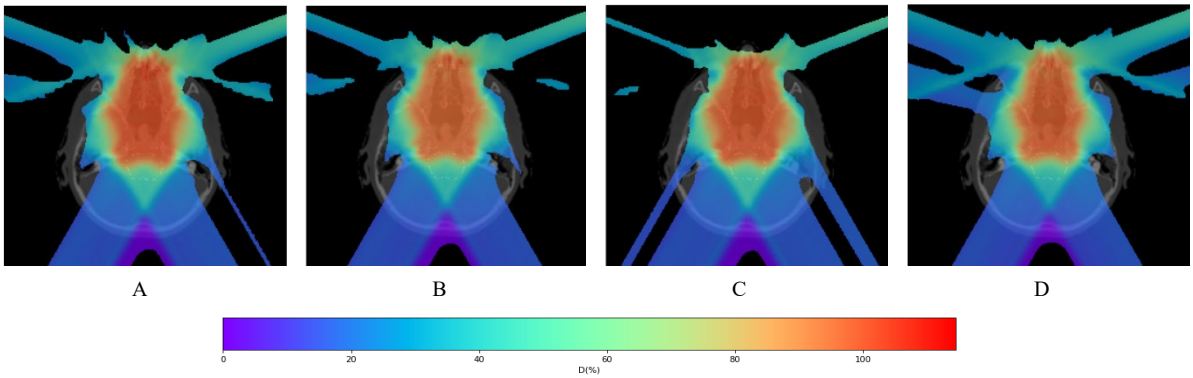

Figure 29: Translational setup errors for (0, ± 1.76, 0) – A, B; (0, 0, ± 1.76) – C, D

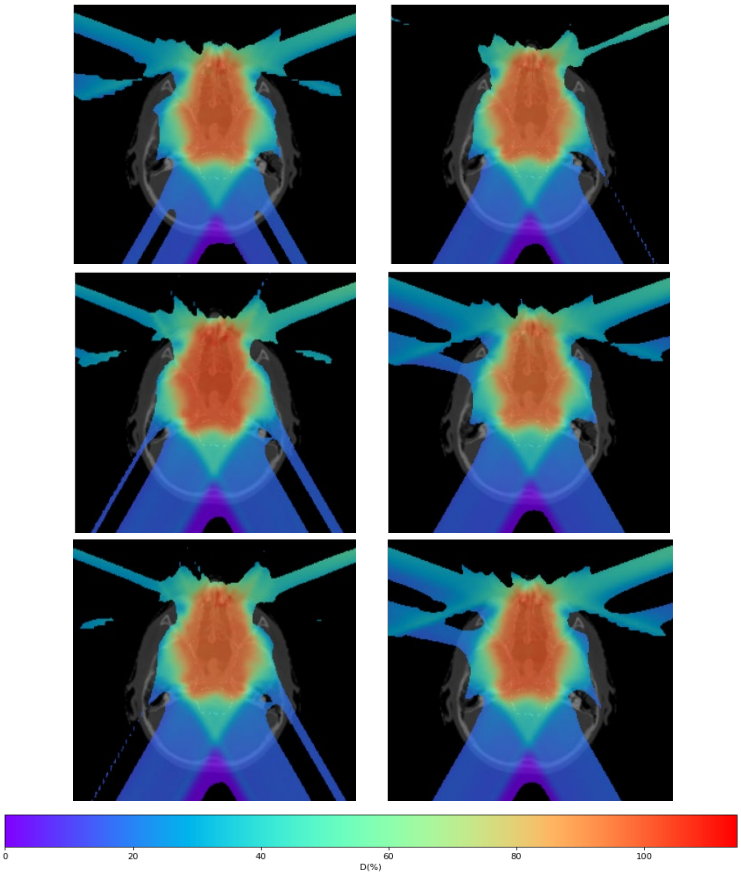

Figure 30: Translational errors for (+ 1.76/√3, + 1.76/√3, −1.76/√3), (− 1.76/√3, − 1.76/√3, +1.76/√3) (top); (− 1.76/√3, + 1.76/√3, +1.76/√3), (+ 1.76/√3, − 1.76/√3, −1.76/√3) (middle); (+ 1.76/√3, − 1.76/√3, +1.76/√3), (− 1.76/√3, + 1.76/√3, −1.76/√3) (bottom)

A.3. Patient C

A.3.1. Rotational setup errors

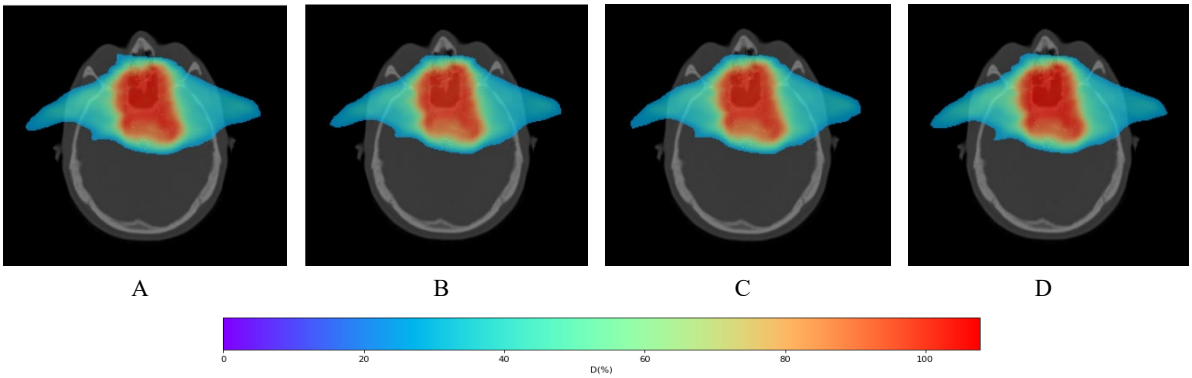

Figure 31: Rotational setup errors for (±1º, 0º, 0º) – A, B; (0º, ±1º, 0º) – C, D;

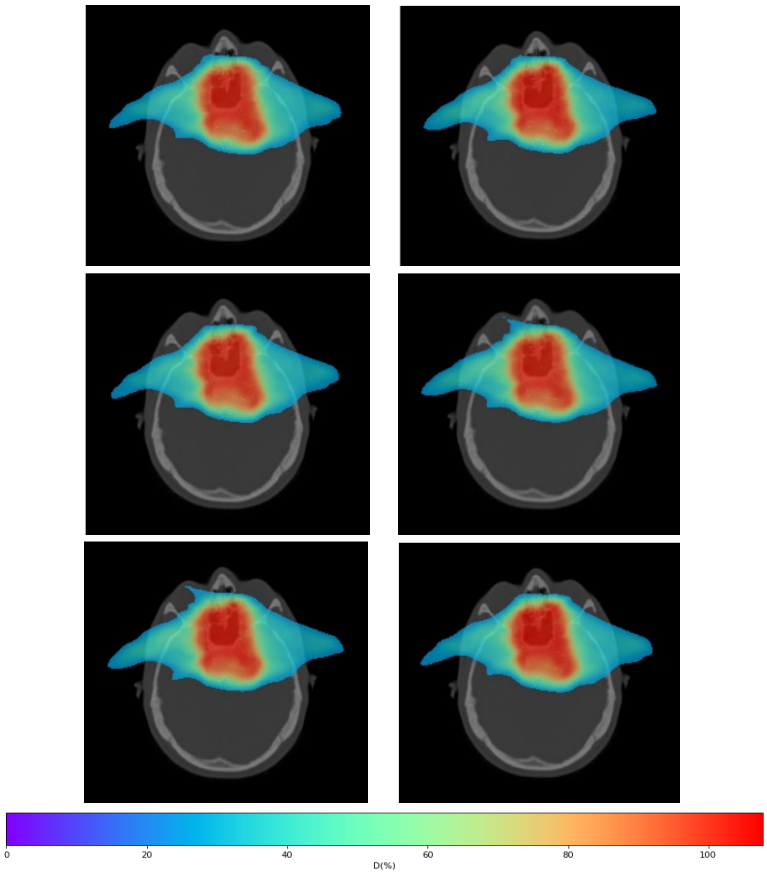

Figure 32: Rotational errors for (+ 1º, + 1º, −1º), (− 1º, − 1º, +1º) (top); (− 1º, + 1º, +1º), (+ 1º, − 1º, −1º) (middle); (+ 1º, − 1º, +1º), (− 1º, + 1º, −1º) (bottom)

A.3.2. Translational shifts

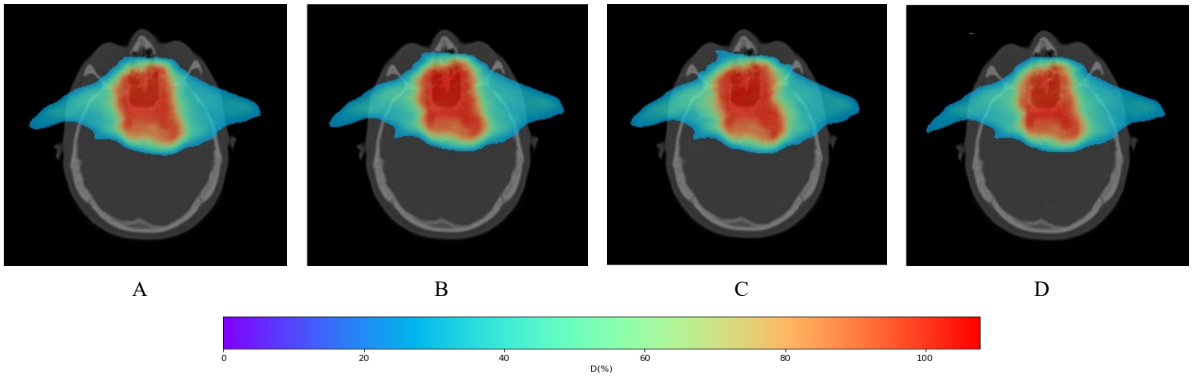

Figure 33: Translational setup errors for (0, ± 1.76, 0) – A, B; (0, 0, ± 1.76) – C, D

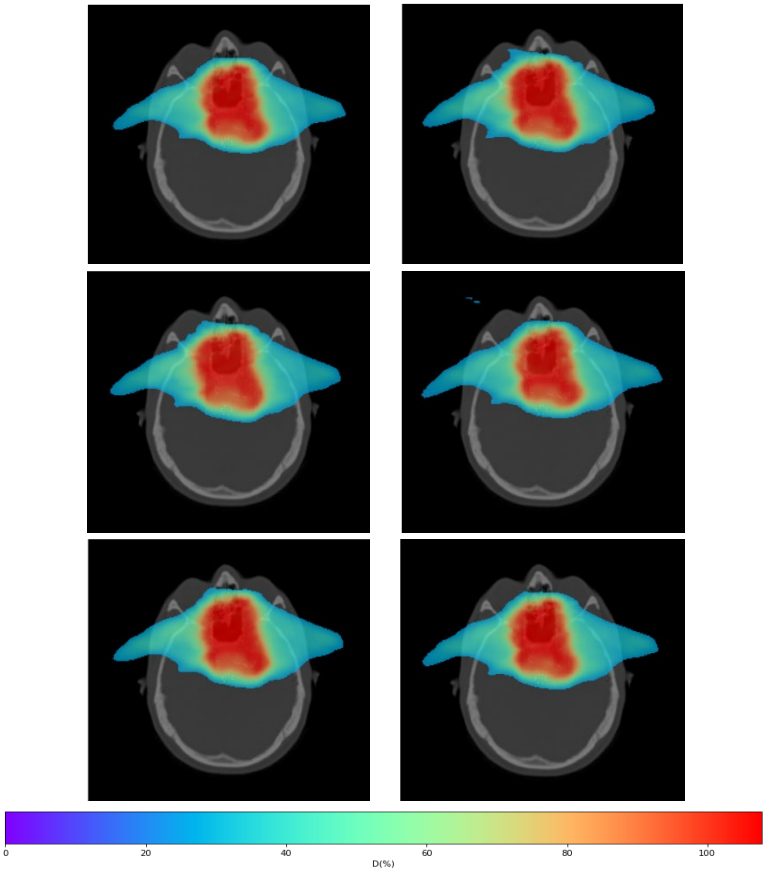

Figure 34: Translational errors for (+ 1.76/√3, + 1.76/√3, −1.76/√3), (− 1.76/√3, − 1.76/√3, +1.76/√3) (top); (− 1.76/√3, + 1.76/√3, +1.76/√3), (+ 1.76/√3, − 1.76/√3, −1.76/√3) (middle); (+ 1.76/√3, − 1.76/√3, +1.76/√3), (− 1.76/√3, + 1.76/√3, −1.76/√3) (bottom)

B. DVH

B.1. Patient A

B.1.1. Rotational setup errors

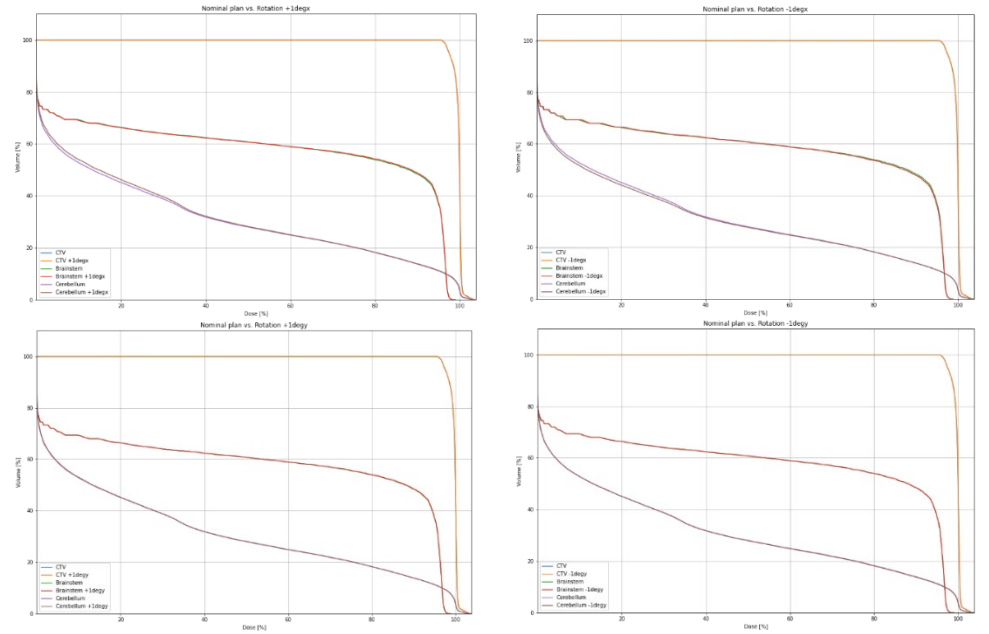

Figure 35: DVH for (±1º, 0º, 0º) (top); (0º, ±1º, 0º) (bottom)

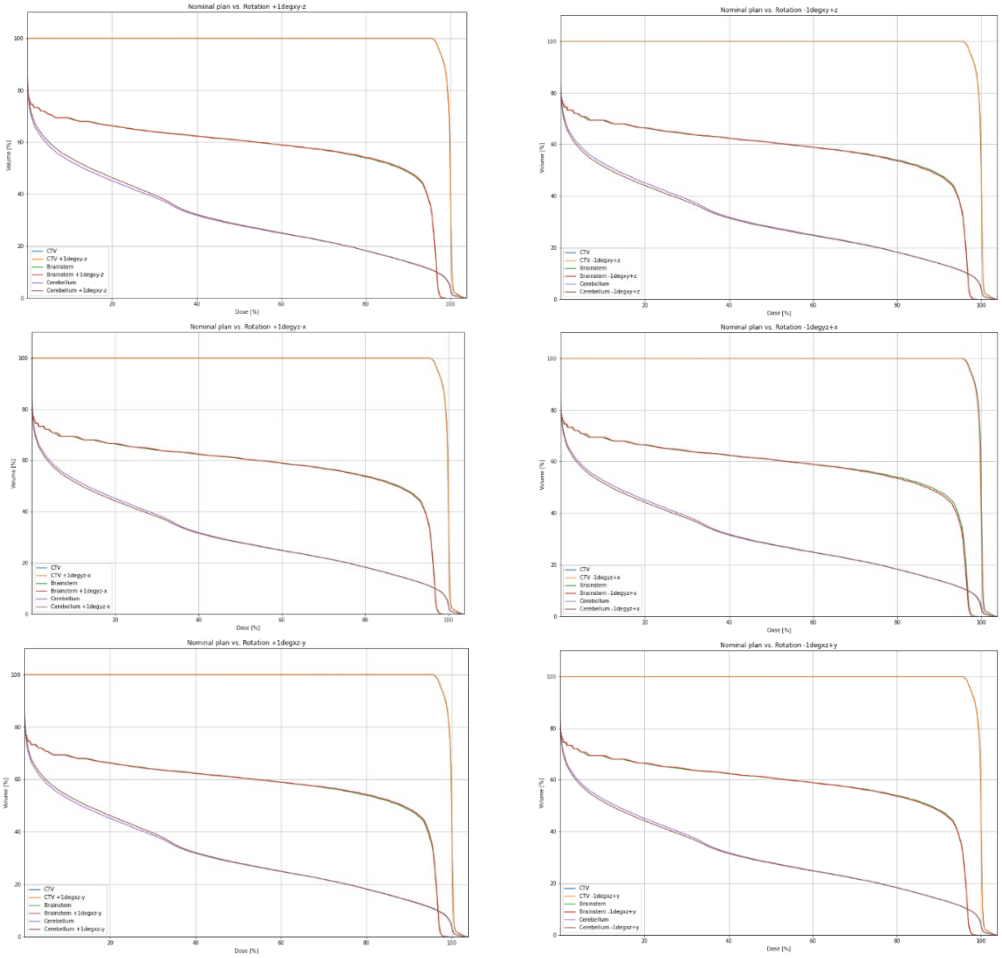

Figure 36: DVH for (+ 1º, + 1º, −1º), (− 1º, − 1º, +1º) (top); (− 1º, + 1º, +1º), (+ 1º, − 1º, −1º) (middle); (+ 1º, − 1º, +1º), (− 1º, + 1º, −1º) (bottom)

B.1.2. Translational setup errors

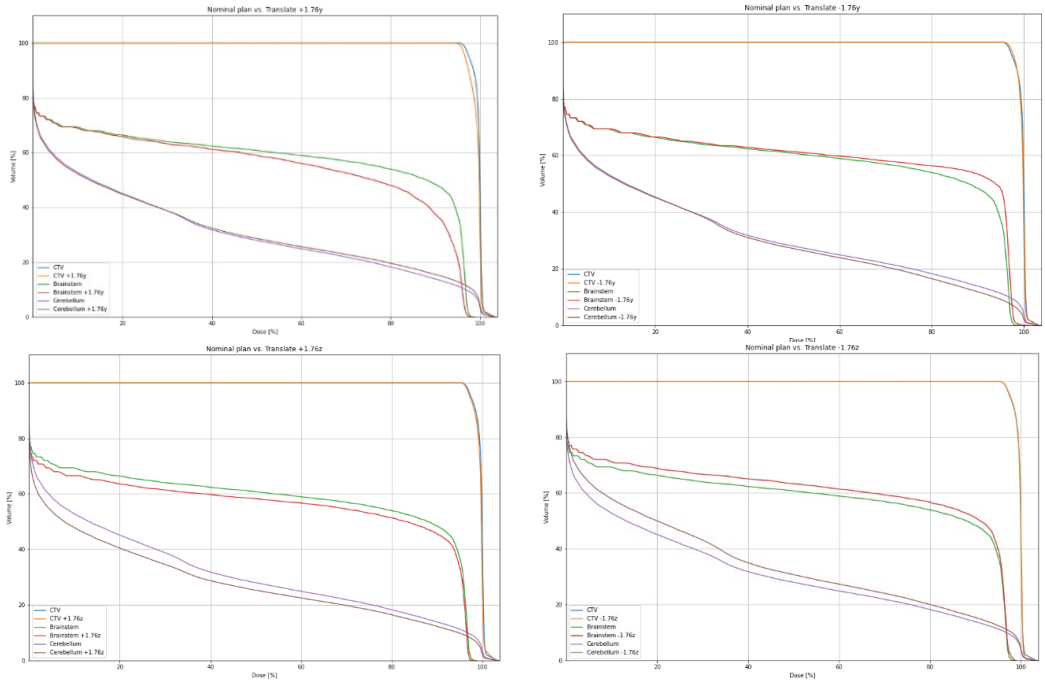

Figure 37: DVH for (0, ± 1.76, 0) (top); (0, 0, ± 1.76) (bottom)

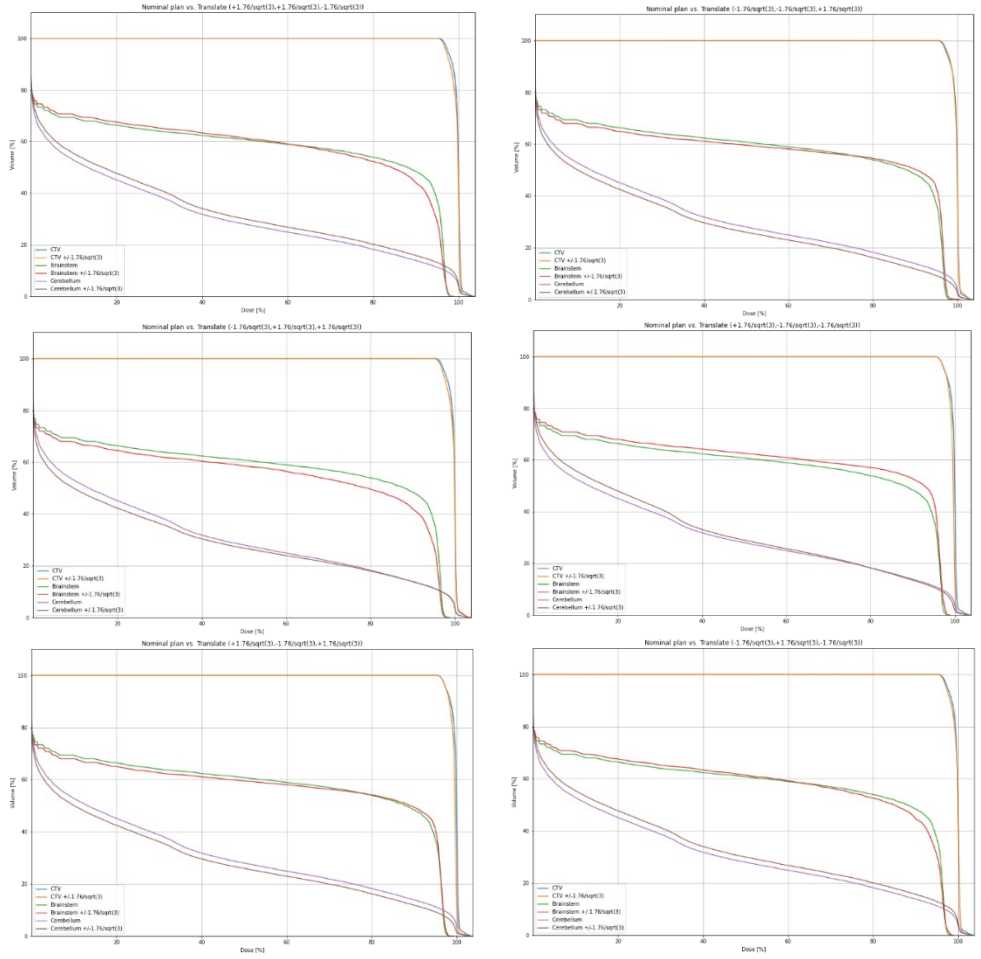

Figure 38: DVH for (+ 1.76/√3, + 1.76/√3, −1.76/√3), (− 1.76/√3, − 1.76/√3, +1.76/√3) (top); (− 1.76/√3, + 1.76/√3, +1.76/√3), (+ 1.76/√3, − 1.76/√3, −1.76/√3) (middle); (+ 1.76/√3, − 1.76/√3, +1.76/√3), (− 1.76/√3, + 1.76/√3, −1.76/√3) (bottom)

B.2. Patient B

B.2.1. Rotational setup errors

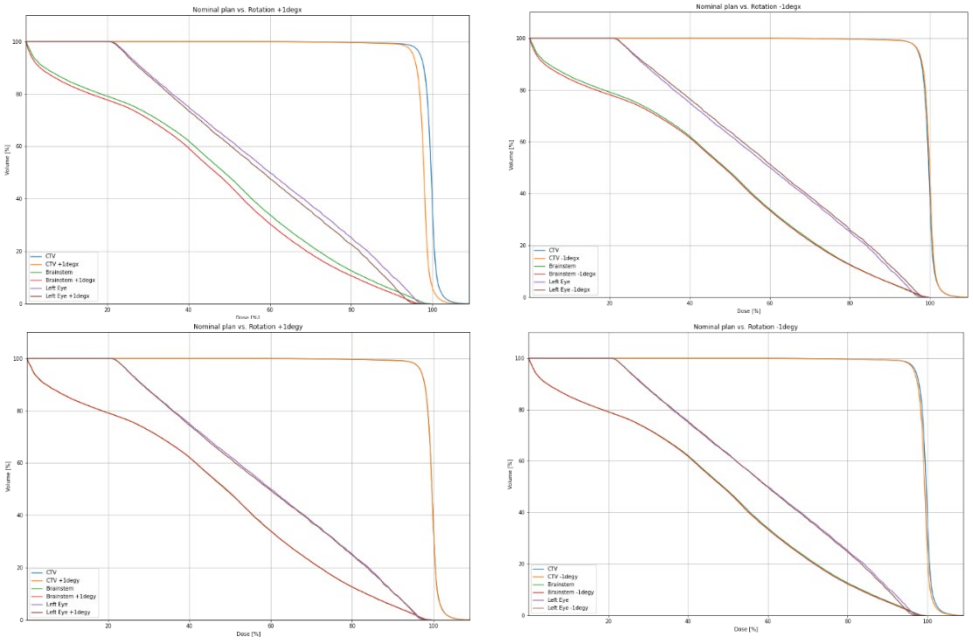

Figure 39: DVH for (±1º, 0º, 0º) (top); (0º, ±1º, 0º) (bottom)

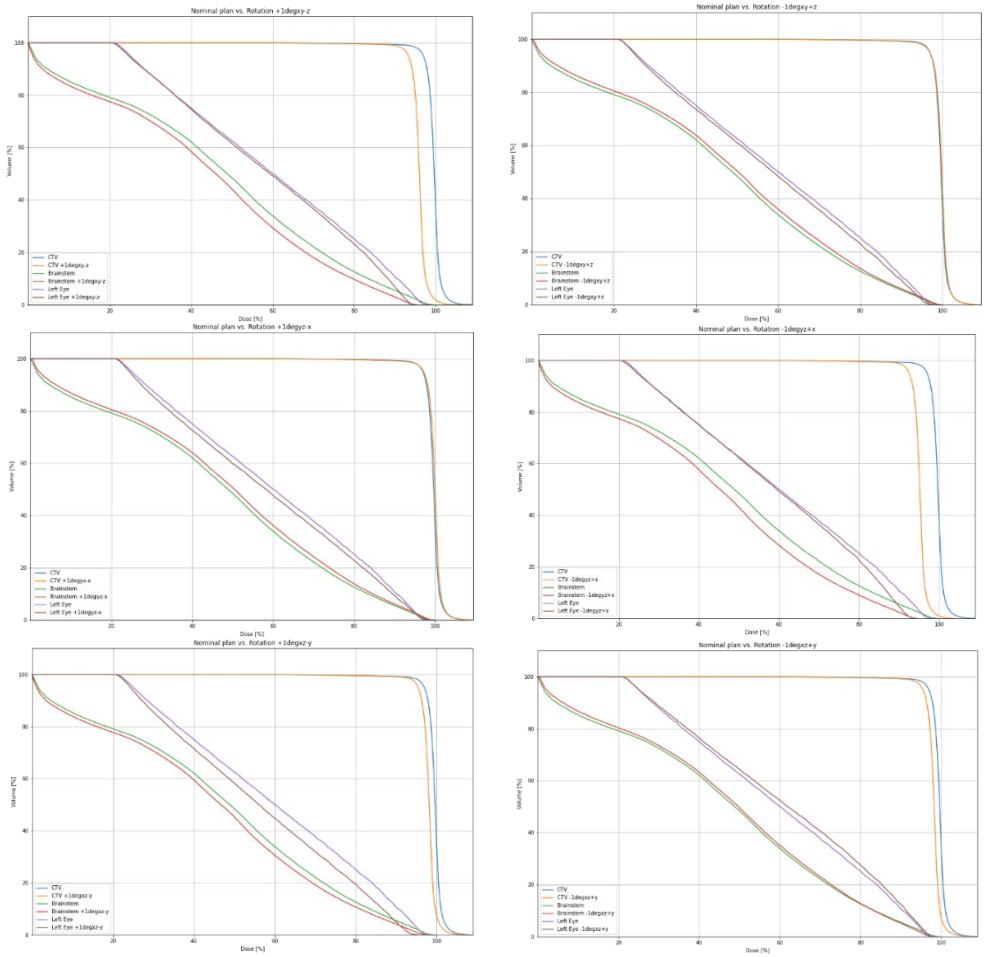

Figure 40: DVH for (+1º, +1º, −1º), (−1º, −1º, +1º) (top); (−1º, +1º, +1º), (+1º, −1º, −1º) (middle); (+1º, −1º, +1º), (−1º, +1º, −1º) (bottom)

B.2.2. Translational setup errors

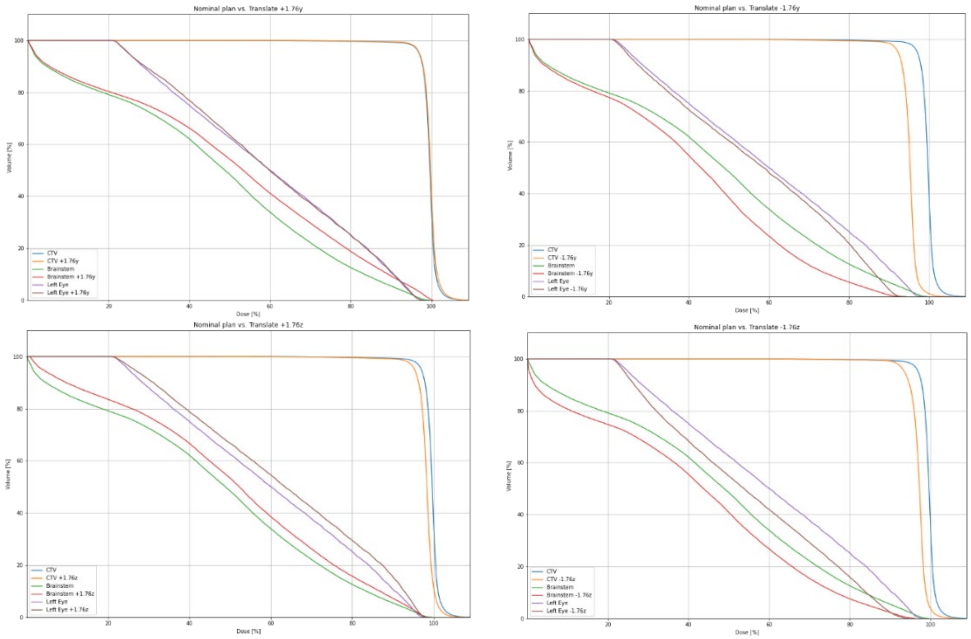

Figure 41: DVH for (0, ± 1.76, 0) (top); (0, 0, ± 1.76) (bottom)

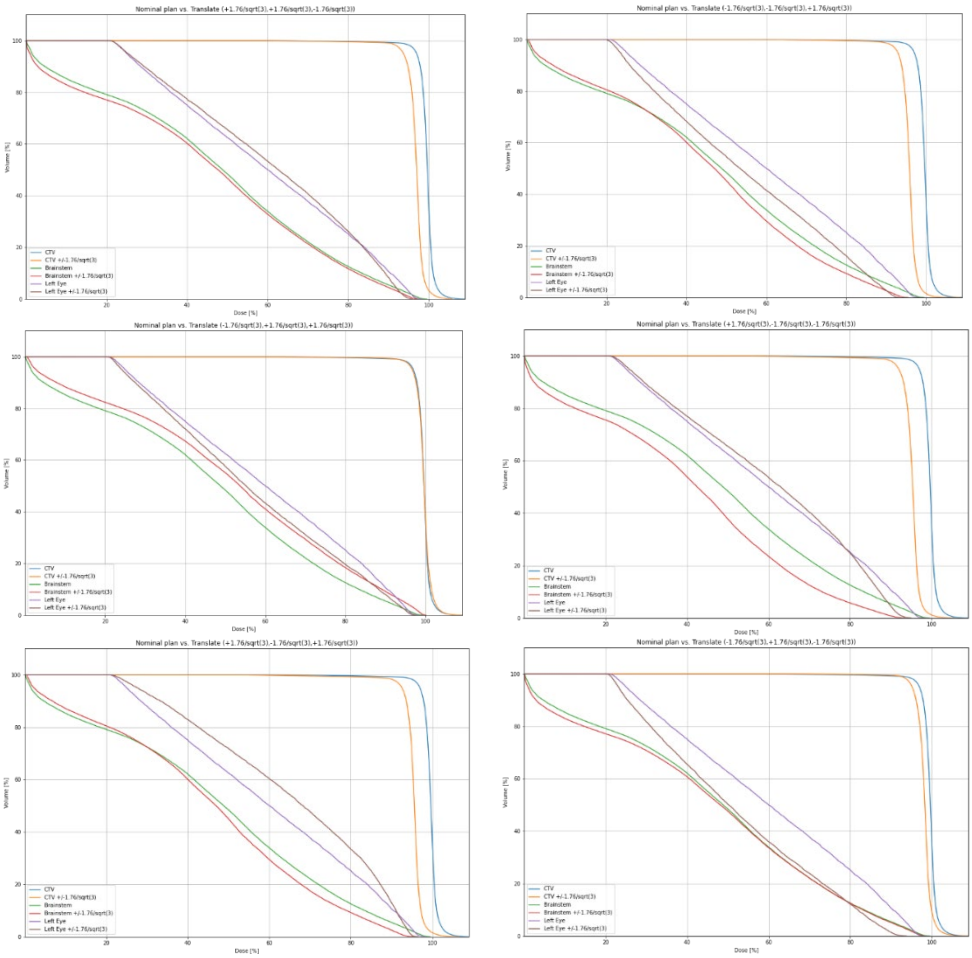

Figure 42: DVH for (+ 1.76/√3, + 1.76/√3, −1.76/√3), (− 1.76/√3, − 1.76/√3, +1.76/√3) (top); (− 1.76/√3, + 1.76/√3, +1.76/√3), (+ 1.76/√3, − 1.76/√3, −1.76/√3) (middle); (+ 1.76/√3, − 1.76/√3, +1.76/√3), (− 1.76/√3, + 1.76/√3, −1.76/√3) (bottom)

B.3. Patient C

B.3.1. Rotational setup errors

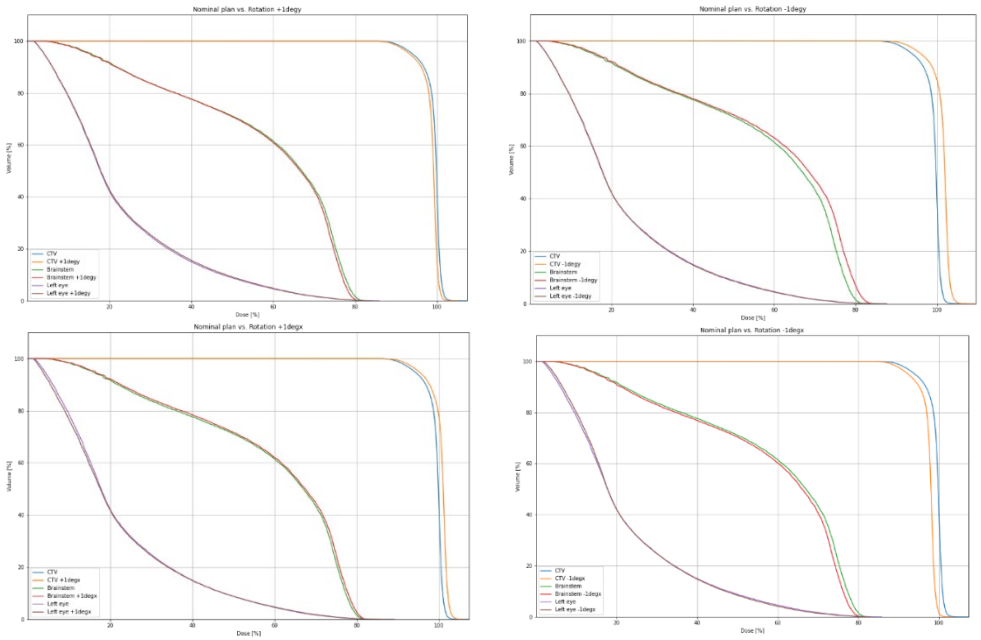

Figure 43: DVH for (±1º, 0º, 0º) (top); (0º, ±1º, 0º) (bottom)

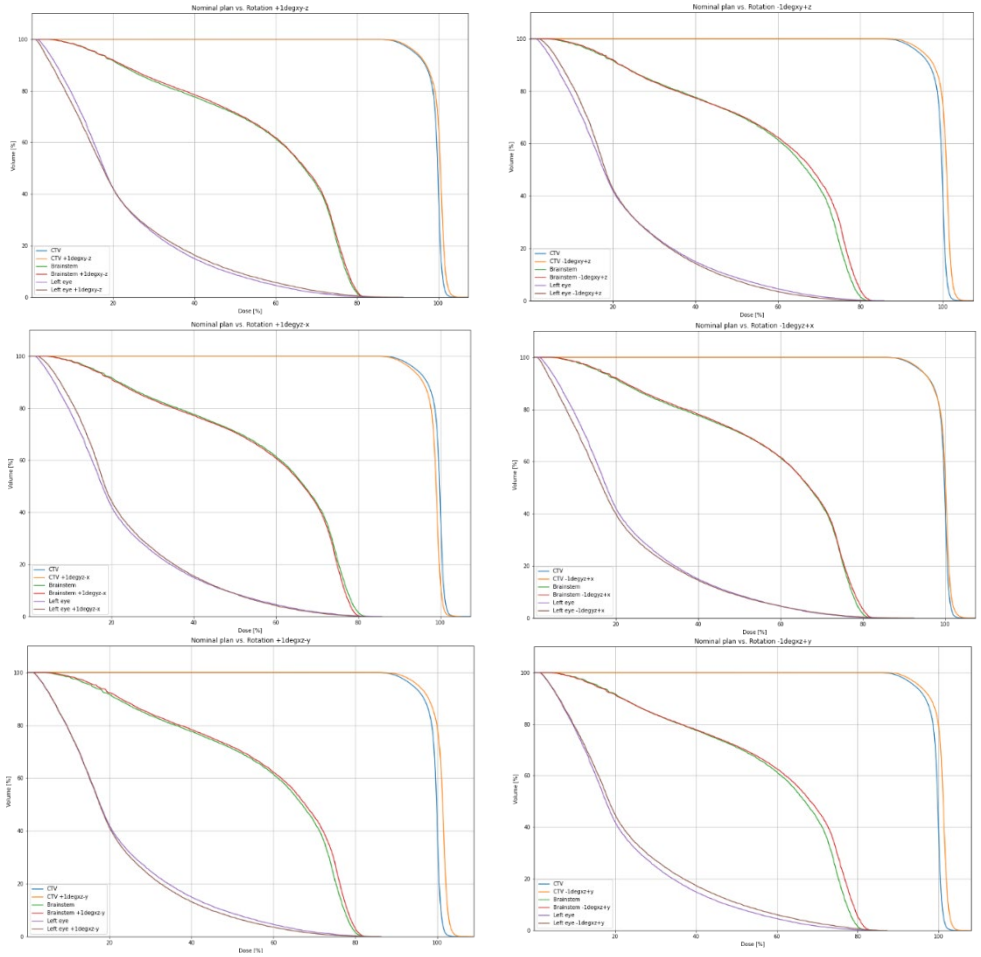

Figure 44: DVH for (+ 1º, + 1º, −1º), (− 1º, − 1º, +1º) (top); (− 1º, + 1º, +1º), (+ 1º, − 1º, −1º) (middle); (+ 1º, − 1º, +1º), (− 1º, + 1º, −1º) (bottom)

B.3.2. Translational setup errors

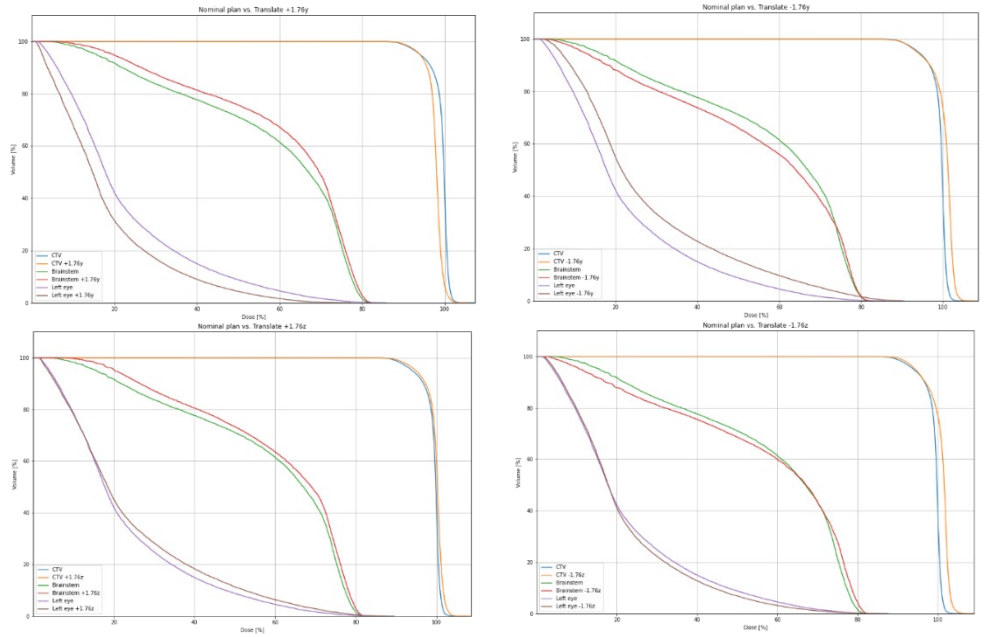

Figure 45: DVH for (0, ± 1.76, 0) (top); (0, 0, ± 1.76) (bottom)

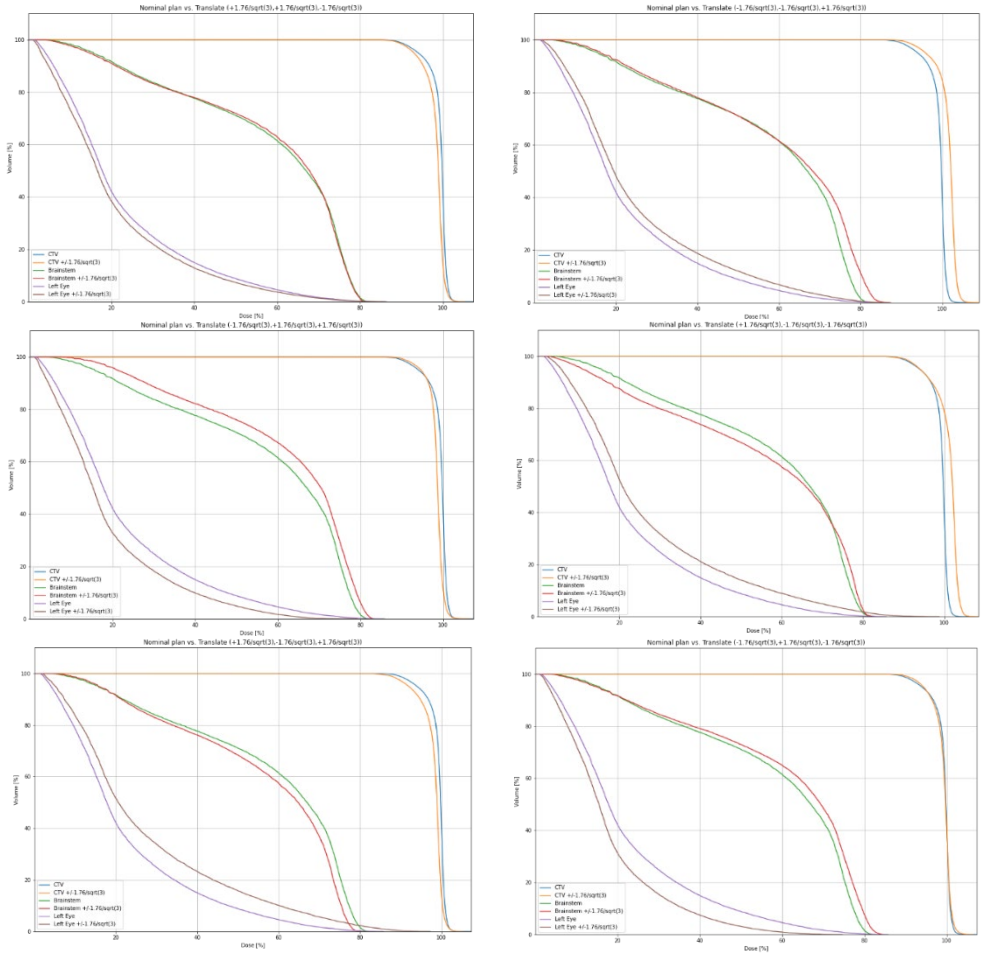

Figure 46: DVH for (+ 1.76/√3, + 1.76/√3, −1.76/√3), (− 1.76/√3, − 1.76/√3, +1.76/√3) (top); (− 1.76/√3, + 1.76/√3, +1.76/√3), (+ 1.76/√3, − 1.76/√3, −1.76/√3) (middle); (+ 1.76/√3, − 1.76/√3, +1.76/√3), (− 1.76/√3, + 1.76/√3, −1.76/√3) (bottom)

C. Worst – case distribution

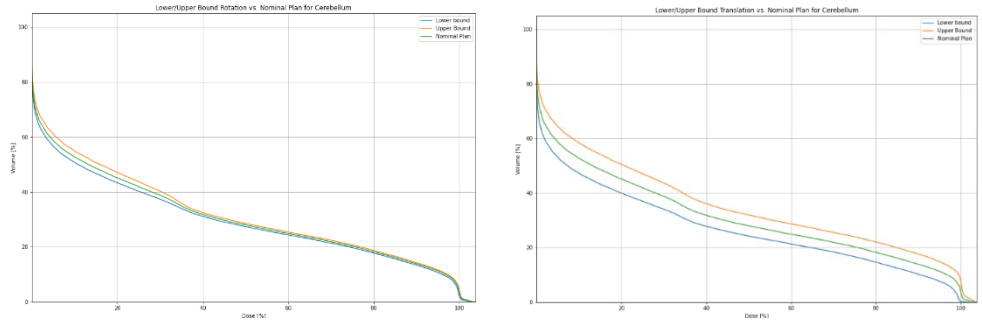

Figure 47: Patient 1 - DVH for the cerebellum showing the lower and upper bound on the treatment plan quality: rotational uncertainties (left) and translational uncertainties (right)

Table 6: D_2 values for the cerebellum in the case of rotational and translational setup uncertainties

	Cerebellum D_2 (Gy_{RBE})					
	Rotational positioning uncertainties			Translational setup uncertainties		
Cases	Best – case	Nominal plan	Worst – case	Best – case	Nominal plan	Worst – case
1	101% (1.81)			99% (1.77)	101% (1.81)	101.5% (1.82)

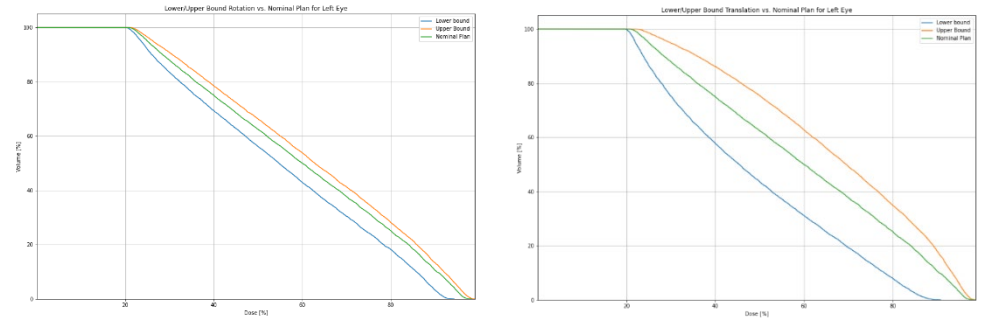

Figure 48: Patient 2 - DVH for the left eye showing the lower and upper bound on the treatment plan quality: rotational uncertainties (left) and translational uncertainties (right)

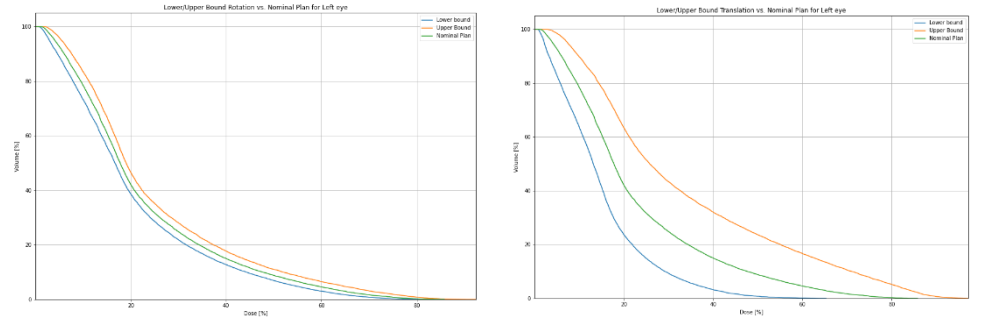

Figure 49: Patient 3 - DVH for the left eye showing the lower and upper bound on the treatment plan quality: rotational uncertainties (left) and translational uncertainties (right)

Table 6: D_2 values for the left eye in the case of rotational and translational setup uncertainties

	Left Eye D_2 (Gy_{RBE})					
	Rotational positioning uncertainties			Translational setup uncertainties		
Cases	Best – case	Nominal plan	Worst – case	Best – case	Nominal plan	Worst – case
2	89% (1.62)	96.4% (1.76)	97% (1.77)	83% (1.51)	96.4% (1.76)	97% (1.77)
3	65% (1.32)	71% (1.45)	76% (1.55)	45% (0.91)	71% (1.45)	87% (1.77)

D. Error bar volume histograms

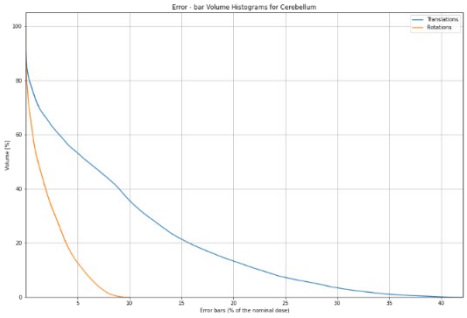

Figure 50: DVH for the cerebellum, corresponding to first patient

Table 8: Error bar values for the cerebellum in the case of rotational and translational setup uncertainties

	$E_{2\%}$	
Cases	Rotational positioning uncertainties	Translational setup uncertainties
A	> 8%	> 35%

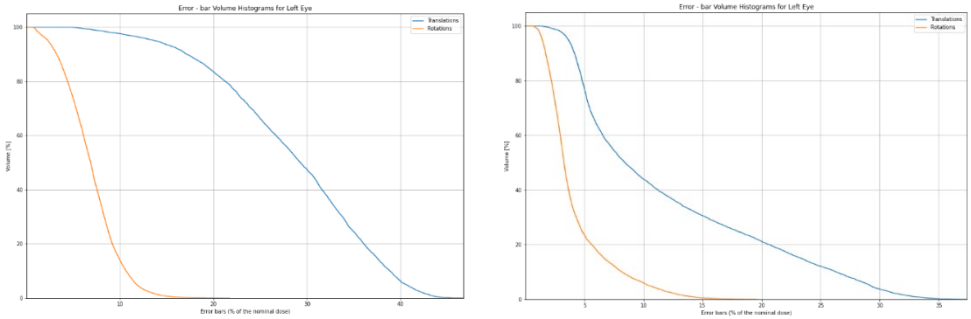

Figure 51: EVH for the left eye, corresponding to the second patient (left) and third patient (right)

Table 9: Error bar values for the left eye in the case of rotational and translational setup uncertainties

	$E_{2\%}$	
Cases	Rotational positioning uncertainties	Translational setup uncertainties
B	> 14%	> 42%
C	> 13.5%	> 33%

Eidgenössische Technische Hochschule Zürich
Swiss Federal Institute of Technology Zurich

Declaration of originality

The signed declaration of originality is a component of every semester paper, Bachelor's thesis, Master's thesis and any other degree paper undertaken during the course of studies, including the respective electronic versions.

Lecturers may also require a declaration of originality for other written papers compiled for their courses.

I hereby confirm that I am the sole author of the written work here enclosed and that I have compiled it in my own words. Parts excepted are corrections of form and content by the supervisor.

Title of work (in block letters):

AN INVESTIGATION INTO THE ROBUSTNESS OF PROTON THERAPY TREATMENTS AGAINST ROTATIONAL AND TRANSLATIONAL SETUP ERRORS

Authored by (in block letters):
For papers written by groups the names of all authors are required.

Name(s):	**First name(s):**
PAUNOIU	ALINA
LOMAX	ANTONY
FATTORI	GIOVANNI

With my signature I confirm that
- I have committed none of the forms of plagiarism described in the 'Citation etiquette' information sheet.
- I have documented all methods, data and processes truthfully.
- I have not manipulated any data.
- I have mentioned all persons who were significant facilitators of the work.

I am aware that the work may be screened electronically for plagiarism.

Place, date

ZÜRICH, 04.01.2023

Signature(s)

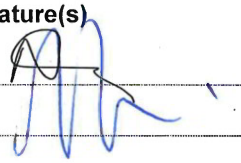

For papers written by groups the names of all authors are required. Their signatures collectively guarantee the entire content of the written paper.